SI Appendix

Evolutionary strata on young mating-type chromosomes despite the lack of sexual antagonism

Sara Branco[1,a], Hélène Badouin[1,a,b], Ricardo C. Rodríguez de la Vega[1a], Jérôme Gouzy[b], Fantin Carpentier[a], Gabriela Aguileta[a], Sophie Siguenza[b], Jean-Tristan Brandenburg[a], Marco A. Coelho[c], Michael E. Hood[2,d], Tatiana Giraud[2,a,*]

[1] These authors contributed equally to the study

[2] These authors jointly supervised the study

[a] Ecologie Systématique Evolution, Bâtiment 360, Univ. Paris-Sud, AgroParisTech, CNRS, Université Paris-Saclay, 91400 Orsay, France.
[b] LIPM, Université de Toulouse, INRA, CNRS, 31326 Castanet-Tolosan, France.
[c] UCIBIO-REQUIMTE, Departamento de Ciências da Vida, Faculdade de Ciências e Tecnologia, Universidade NOVA de Lisboa, 2829-516 Caparica, Portugal.
[d] Department of Biology, Amherst College, 01002-5000 Amherst, Massachusetts, United State of America.

* Corresponding author: Tatiana Giraud (tatiana.giraud@u-psud.fr)

SI Appendix Includes:

SI Text

Mating-type chromosomes in fungi

There are several hypotheses for the evolution of recombination suppression in fungal mating-type chromosomes, some also holding for animal, plant and algal sex chromosomes. These include:

1) Linkage of two mating-type loci: Most basidiomycete fungi (i.e., mushrooms, rusts and smut fungi) contain two loci determining pre- and post-mating compatibility, respectively. The PR locus controls gamete fusion, with pheromone receptor and pheromone precursor genes (the latter sometimes being present in multiple copies), and the HD locus controls compatibility during growth of after fusion of haploids cells, with two adjacent homeodomain genes (1, 2 , 3). Both PR and HD mating-type loci in basidiomycetes encompass two to several genes, and recombination is suppressed within each of these two loci, in all species, ensuring proper mating-type determination (3, 4). Linkage of these two mating-type loci is beneficial (but not required) under selfing mating systems in basidiomycete fungi as it increases the probability of compatibility among gametes from the same diploid parent (5-7) (Fig. S2). In contrast, the segregation of the two mating-type loci in association with multi-allelism increases discrimination against selfing and mating among closely related individuals, which promotes outcrossing (5-9). The PR and HD loci segregate independently in most basidiomycetes, but these loci are linked in some species (6, 10-13). Independent meiotic segregation of the two mating-type loci in basidiomycetes is called tetrapolarity (because meiotic segregation can result in four possible mating types among gametes of a diploid parent, Fig. S2A), while linkage of the mating-type loci in basidiomycetes leads to bipolarity (segregation of only two mating types among gametes of a diploid parent, Fig. S2C).

2) A second explanation for suppressed recombination in fungal mating-type chromosomes is the linkage of mating-type genes to the centromere. In ascomycete and basidiomycete automictic species (*i.e.,* undergoing selfing among products of the same meiotic tetrad (11, 14, 15)), such linkage is particularly common and thought to be favorable (16, 17), resulting in mating-type segregation and reformation of the diploid between meiotic products separated at the first meiotic division. In basidiomycetes, linkage of both HD and PR mating-type genes to their respective centromeres increases the odds of compatibility within tetrads (Fig. S2B). Note that in basidiomycete fungi with linked HD and PR genes, linkage to the centromere is not beneficial with regard to the odds of compatibility between gametes, as it will not further increase mating compatibility among gametes in a diploid individual (Fig. S2C).

3) In analogy to the sexually antagonistic selection hypothesis, which is the main theory for explaining evolutionary strata in sex chromosome evolution, there could be "mating-type antagonistic selection" (18) if some phenotypes were beneficial for improving the a_1 function while being detrimental

to the a_2 function, or vice versa. However, there are not many traits that could have different optima in the two mating types.

4) Epistatic interactions can also favor linkage for protecting beneficial combinations of alleles, unrelated to mating type or sex functions. Unlike hypothesis 3 above that also deals with epistasis (19), this fourth hypothesis postulates that beneficial allelic combinations do not improve the a_1 and a_2 mating type functions in themselves, and therefore does not correspond to "mating-type antagonistic selection". Epistatic interactions can also occur on autosomes but the maintenance of alternative alleles should be facilitated when linked to the mating-type or sex-determining genes, which are under strong balancing selection.

5) Another evolutionary explanation for suppressed recombination on fungal mating-type chromosomes, that could also apply to sex chromosomes, involves linkage of deleterious alleles to the mating-type loci, favoring permanent sheltering in an heterozygous state, as has been theoretically modeled (20, 21). This may arise specifically in sex and mating-type chromosomes if recombination frequency gradually decreases from the non-recombining into the PAR, so that partial linkage (linkage disequilibrium) to mating-type or sex-determining genes makes selection against recessive deleterious alleles less efficient. This would allow deleterious alleles to increase in frequency in these PAR edges at the margin of the non-combining region. Rare recombination events would then generate individuals homozygous for deleterious alleles and could therefore be selected against. Complete linkage of these PAR margins in disequilibrium with mating type may thus be favorable and selected for (Fig. S1A). Permanent sheltering would thus be more easily achieved than purging if recombination is rare at the PAR margins. Further theoretical models are needed to explore the general conditions under which such a mechanism can generate evolutionary strata.

6) A last mechanism explaining suppressed recombination involves neutral inversions or rearrangements extending the region of suppressed recombination (22); these could be fixed by drift in one of the sex or mating-type chromosomes and arrest recombination between sex or mating-type chromosomes. For example, an inversion trapping a part of the PAR at the margin of the non-recombining region could be neutral in the short term, and could be fixed by drift in one of the sex or mating-type chromosomes, and not the other, because of the recombination suppression and because of mating occurring only between mating types (Fig. S1B and C). Such phenomena can occur on any chromosome, but linkage in mating-type and sex chromosomes could be maintained longer in a polymorphic state (and therefore be more detectable), due to balancing selection retaining alternate alleles determining sexes and mating types (22). As for the hypothesis above, theoretical models could be developed for validating whether such a mechanism can generate evolutionary strata.

The *Microbotryum lychnidis-dioicae* system

Contributing to understanding of these various evolutionary models, the anther-smut fungus *Microbotryum lychnidis-dioicae* has been important for the study of fungal mating-type chromosomes. It was central to the first studies describing bipolar breeding systems in fungi (23) and the first case of size-dimorphic mating-type chromosomes in fungi (24). Suppressed recombination encompasses ca. 90% of the mating-type chromosome lengths (sized 3.5 Mb for a_1 and 4.0 Mb for a_2) with 614 and 683 predicted non-transposable element genes, respectively (12, 24-27). The non-recombining region shows chaos of rearrangements and gene losses, transposable element accumulation, non-synonymous substitutions and impaired gene expression (12, 27). The non-recombining region is flanked at both sides by two small recombining and collinear regions, therefore called pseudo-autosomal regions (PARs).

The existence of evolutionary strata has been debated in *M. lychnidis-dioicae.* Varying levels of synonymous divergence between a_1 and a_2 alleles in a handful of genes in the unassembled non-recombining region led to the claim that evolutionary strata existed (28). Based on highly fragmented assemblies, it was then speculated that an oldest stratum evolved for linking pheromone precursor and pheromone receptor genes, a second small (60 kb) old stratum for linking the HD and PR locus, and a third recent and large stratum for linking the MAT genes to the centromeres (29). However, the full assemblies of the mating-type chromosomes recently showed that the HD and PR locus are 600 kb apart, that no clear discrete strata patterns were discernable using the current gene orders, as genes with different a_1-a_2 synonymous divergence levels (a proxy for time since recombination suppression) were dispersed chaotically along the chromosomes (12). These observations could be explained by a lack of evolutionary strata, extensive rearrangements of original strata, and/or gene conversion, which is known to occur in fungal mating-type chromosomes (30, 31). A recent study suggested the existence of five evolutionary strata along the mating-type chromosomes in *M. lychnidis-dioicae* using a clustering method based on putative oligonucleotide compositional differences between strata (32); however, this method did not seem to yield reliable inference because it could not retrieve the pseudo-autosomal boundary in one mating-type chromosome. Furthermore, each inferred stratum included genes with highly heterogeneous levels of divergence (12). Our study shows that the recovered putative strata in this previous study (32) in fact did not correspond to genuine evolutionary strata.

Elucidating whether evolutionary strata exist and which genomic regions they include is important for understanding how and why suppressed recombination evolved. The different mechanisms for explaining suppression of recombination outlined above do not all predict the existence of evolutionary strata. For example, linking the two mating-type loci would not generate multiple strata, while the successive linkage of deleterious alleles to the mating-type locus would (20). In this regard, an interesting feature of *M. lychnidis-dioicae* is that frequent deleterious alleles linked to mating types have been reported, that prevent haploid growth (14, 33, 34). In fact, many genes have been lost from

one or the other mating type (12) and transposable elements and non-synonymous substitutions have accumulated in non-recombining regions (12, 27).

Genome assemblies and comparisons

We used Pacific Bioscience sequencing technologies to generate very high quality genome assemblies for the mating-type chromosomes of several *Microbotryum* species. The a_1 and a_2 haploid genomes of *M. lagerheimii* and one haploid genome of *M. intermedium* were well assembled, with 42 and 37 contigs for a_1 and a_2 *M. lagerheimii*, respectively, 24 contigs for *M. intermedium*, for an estimated number of chromosomes of 12 for haploid *Microbotryum* genomes (24). The mating-type chromosomes were well assembled; the HD chromosomes of *M. intermedium* and *M. lagerheimii* appeared assembled in a single contig each, and were homologous and syntenic between the species; the complete PR chromosome of *M. intermedium* matched two contigs in the a_1 *M. lagerheimii* assembly, with a small inversion internal to one contig (the MC16 contig, in dark purple in Figure 2A; the inversion is represented by the orange links).

In addition to collinearity with *M. intermedium*, collinearity between the a_1 and a_2 mating-type chromosomes within *M. lagerheimii* (Fig. S4) indicates that recombination is frequent enough to conserve gene order along most of their lengths. In *M. lychnidis-dioicae* the recombining pseudo-autosomal regions of the mating-type chromosomes and autosomes are also highly collinear between a_1 and a_2 genomes, while the non-recombining regions of the mating-type chromosomes are thoroughly rearranged (Fig. S3).

The two distinct contigs carrying the PR and HD genes in *M. lagerheimii* (Fig. S4) are consistent with the species being tetrapolar, as inferred earlier based on meiotic segregation analysis of recombination between these mating-type loci (35). The high degree of collinearity between the mating-type chromosomes of *M. lagerheimii* and *M. intermedium*, and the finding of PR and HD genes in different contigs, each harbouring centromere-specific repeats (12) (Fig. 2A), indicate that *M. intermedium* is also tetrapolar.

We included comparisons of the mating-type chromosomes of *M. lychnidis-dioicae* and *M. violaceum s. str.* (Fig. S5B), whose haploid genomes were also well assembled (Table S4). Three contigs in the a_1 *M. violaceum sens. str.* genome matched the a_1 mating-type chromosomes of *M. lychnidis-dioicae*. In addition, these three contigs had some fragments joined together in the assembly of the *M. violaceum sens. str.* a_2 genome (Fig. S5D), indicating that all three belonged to the mating-type chromosome. The non-recombining region was highly rearranged between *M. lychnidis-dioicae* and *M. violaceum s. str.* (Fig. S5B) in all four possible comparisons, as well as between a_1 and a_2 in both species (Fig. S5D).

We also compared the mating-type chromosomes of the sister species *M. lychnidis-dioicae* and *M. silenes-dioicae* (Fig. S5C), the latter being assembled in more contigs than other species (Table S4;

6 contigs for both a_1 and a_2 mating-type chromosomes). These different contigs had some fragments joined together in the assembly of the alternative mating type (Fig. S5E) and in *M. lychnidis-dioicae* (Fig. S5C), allowing assigning to mating-type chromosomes. The non-recombining region appeared homologous but already highly rearranged between *M. lychnidis-dioicae* and *M. silenes-dioicae* (Fig. S5C) in all four possible comparisons, as well as between a_1 and a_2 in *M. silenes-dioicae* (Fig. S5E).

SI Materials and Methods

DNA extraction and sequencing

DNA was extracted using the Qiagen Kit 10243 (Courtaboeuf, France) following manufacturer instructions and using a Carver hydraulic press (reference 3968, Wabash, IN, USA) for breaking cell walls. A haploid genome of *M. intermedium* (strain 1389-BM-12-12, collected on *Salvia pratensis*, Italy, Coord. GPS : 44.33353 & 7.13637), as well as the genomes of a_1 and a_2 haploid cells of *M. lagerheimii* (strain 1253, collected on *S. vulgaris*, near Chambery, France, Coord. GPS : 45.4 & 6.11), *M. violaceum s. str*. (strain 1249, collected on *S. nutans*, Guarda, Switzerland, Coord. GPS : 46.777 & 10.16) and *M. silenes-dioicae* (strain 1303, collected on *S. dioica*, Bois Carre, Lac de Puy Vachier 45.026485 & 6.276612) were sequenced using the P6/C4 Pacific Biosciences SMRT technology (UCSD IGM Genomics Facility La Jolla, CA, USA) (Table S4).

Assembly and annotation

We assembled the haploid genomes of a_1 and a_2 *M. lagerheimii, M. violaceum s. str., M. silenes-dioicae,* and a_1 *M. intermedium*, and re-assembled the reference genome of *M. lychnidis-dioicae* Lamole (12) into separated a_1 and a_2 haploid genomes. Assemblies of the genomes were generated with the wgs-8.2 version of the PBcR assembler (36) with the following parameters: genomeSize=30000000, assembleCoverage=50. Assemblies were polished with quiver software (https://github.com/PacificBiosciences/GenomicConsensus). A summary of raw data and assembly statistics is reported in Table S4.

The protein-coding gene models were predicted with EuGene (37), trained for *Microbotryum*. Similarities to the fungi subset of the uniprot database (38) plus the *M. lychnidis-dioicae* Lamole proteome (12) were integrated into EuGene for the prediction of gene models.

Mating-type chromosomes were identified by: 1) finding the contigs carrying the PR or HD mating-type genes in both a_1 and a_2 haploid genomes, 2) using BLAST to search the a_1 against the a_2 haploid genomes and visualizing the output using Circos (39) for identifying contigs with lack of collinearity, 3) blasting the haploid genomes against the completely assembled mating-type chromosomes of *M. lychnidis-dioicae* (12), 4) blasting the a_1 contigs identified in the first steps to the whole a_2 haploid genome, and reciprocally, to identify additional mating-type contigs, 5) repeating this process from step 3 until no additional contig was identified. These contigs were then orientated by: 1) using the centromere-specific repeats (12), as initial assemblies often yielded chromosome arms broken at their centromeres, with identifiable centromere-specific repeats on each separated contig (e.g., Fig. 2A); and 2) blasting the a_1 and a_2 mating-type contigs against each other for identifying the PARs as the collinear regions, that were then assumed to be at the edges of the chromosomes. When the mating-type

chromosomes were fragmented and internal contigs did not include centromeric repeats at one of its edges, it was impossible to recover contig orientation (as indicated in the figure captions).

Figures and statistical tests

The Figures 2, S3, S4 and S5 were prepared using Circos (39). We analyzed gene order to identify larger blocks of synteny. Alleles were assigned between the two mating-type chromosomes and between species by applying orthomcl (40) to the protein data sets. The Student t test was performed using JMP v7 (SAS Institute).

Species tree

We compared the translated gene models of five *Microbotryum* species and the red yeast *Rhodotorula babjevae* with blastp+ 2.30, and the output was used to obtain orthologous groups by Markov clustering (41) as implemented in OrthoMCL v1.4 (40). We aligned the protein sequences of 4,000 single-copy autosomal genes with MUSCLE v3.8.31 (42), and obtained the codon-based CDS alignments with TranslatorX (43). We used RAxML 8.2.7 (44) to obtain maximum likelihood gene trees for all 4,000 fully conserved single-copy genes and a species tree with the concatenated alignment of 2,100,301 codons with no gaps (trimal -nogaps option (45)) under the GTRGAMMA substitution model. We estimated the branch support values by bootstrapping the species tree based on the concatenated alignment and by estimating the relative internode and tree certainty scores based on the frequency of conflicting bipartitions for each branch in the species tree among the fully conserved single-copy genes (46).

Gene genealogies

Gene genealogies were inferred for codon-based alignments of genes in the different strata using RAxML (44) version 8.2.7, assuming the GTRGAMMA model and rapid bootstrap (options: -f a and -# 100). We analyzed for trans-specific polymorphism levels all single-copy genes for which we had both alleles and all species.

Date estimates for recombination suppression

In order to estimate dates of recombination suppression, we leveraged the codon-based alignments of single-copy orthologous groups yielding gene trees displaying trans-specific polymorphism in each evolutionary stratum, as the divergence between alleles associated to the a_1 versus a_2 mating types then corresponds to the time since recombination suppression. We could use three gene families in the purple stratum (1,744 aligned codons), 22 gene families in the black stratum (17,776 aligned codons) and four

gene families in the red stratum (2,726 aligned codons), with alignments including the five *Microbotryum* species and the red yeast used as outgroup, and gene genealogies showing trans-specific polymorphism. There was not enough single-copy gene families showing trans-specific polymorphism for reliable date estimate in the other evolutionary strata. Divergence times were estimated using BEAST v2.4.0 (47), the xml inputs being generated using BEAUTi, and setting the following parameters (others left as default values): unlinked substitution (HKY+G with empirical frequencies for each codon position) and clock models, Yule process to model speciation, and 10,000,000 mcmc generations sampled every 1,000. For all runs we used a single calibration prior at 0.42 million years, corresponding to the divergence between *M. lychnidis-dioicae* and *M. silenes-dioicae* (48), with a normal distribution and a sigma of 0.05.

Transposable element identification

Repetitive DNA content was analyzed with RepeatMasker (49), using REPBASE v19.11 (50). For plotting d_S along chromosomes, these repeats were removed and further filtering of repeats was performed by blasting (tBLASTx) and removing those matching at more than five locations in the genome.

Polymorphism data and analyses

To rule out high levels of polymorphism as the cause for the observed high d_S values in the *Microbotryum* mating-type chromosomes, we assessed the level of polymorphism across *M. silenes-dioicae* and *M. lychnidis-dioicae* by using multiple available genomes (Illumina paired-end 60x-100x), from individuals collected across Europe (29, 51). We only used genomes including a single mating-type chromosome (a_1 or a_2) either because a haploid strain was sequenced or because a lethal allele was linked to one mating type in a diploid strain so that only haploid cells carrying the alternative mating-type chromosome could be cultivated *in vitro* and sequenced (34, 51, 52). We compiled sequences for a total of ten a_1 and fourteen a_2 mating-type chromosomes of *M. lychnidis-dioicae*, and six a_1 and eight a_2 mating-type chromosomes of *M. silenes-dioicae* (Table S5).

We used two approaches to determine which mating-type chromosome(s) were present in genomes sequences (a_1 or a_2), by checking the presence/absence of the a_1 and a_2 pheromone receptor alleles. First, each genome was assembled *de novo* using SOAPdenovo (53) with default parameters, and searched using BLAST for the sequences of the pheromone receptor alleles of *M. lychnidis-dioicae* and *M. silenes-dioicae*, which are highly differentiated between a_1 and a_2 (54). In a second validation step, we counted the reads mapped against the two alleles of the mating-type pheromone receptors. Strains that displayed reads mapping against both alleles were excluded from further analyses.

We performed SNP calling as described previously (51). Reads were mapped with GLINT (T. Faraut & E. Courcelle, available at http://lipm-bioinfo.toulouse.inra.fr/download/glint/) with parameters

set as follows: minimum length of the high-scoring pair hsp ≥ 90, with ≤ 5 mismatches, no gap allowed, only best-scoring hits taken into account. For each strain, we used as a reference for mapping the haploid PacBio genome assembly corresponding to its species and mating-type. Between 92% and 97% of reads were mapped as proper pairs, and the mapping coverage ranged from 50 to 171 (Table S5). SNPs were called with VarScan (55) (min-coverage 10, min-reads2 5, min-avg-qual 30, min-var-freq 0.3, p-value 0.01), and filtered to remove SNPs located near indels, strand-biased SNPs and heterozygote SNPs.

To compute statistics of diversity, we generated pseudo-alignments of CDS in FASTA format from the VCF file produced by VarScan as previously (51). Pseudo-alignments are obtained by substituting reference nucleotides by their variants in the reference sequence. We then computed the θ_π statistic of diversity with EggLib version 2 (56) for each species and mating-type.

We generated alignments combining the *M. lychnidis-dioicae* and *M. silenes-dioicae* sequences generated above, as well as sequences of the other species. Codon-based alignments of single-copy genes in mating-type evolutionary strata and autosomes were obtained with MUSCLE and translatorX (see above). We used a custom python script to incorporate the sequences of the multiple genomes of *M. lychnidis-dioicae* and *M. silenes-dioicae* while taking into account gaps in the translatorX alignments. Trees were computed with the RAxML rapid bootstrap mode (-f a -m GTRGAMMA -x -# 100). To help visualization, trees were rooted using *R. babjevae* and *M. intermedium*, and strains were colored by mating-type with the ETE3 python toolkit (57).

For further checking that the observed differences in diversity levels between the pseudo-autosomal regions and the different strata in *M. lychnidis-dioicae* and *M. silenes-dioicae* (SI Appendix, Table S6) were not due to differences in mutation rates, we performed maximum-likelihood Hudson-Kreitman-Agade (MLHKA) tests as implemented in the MLHKA software (58) using the multiple genomes described above. The MLHKA test is designed to detect signatures of departure from neutrality (either balancing or positive selection) while controlling for mutation rate by the use of divergence data, and it allows multilocus comparisons (58). MLHKA tests can thus be used to test whether differences in diversity levels between two sets of genes is most likely due to elevated mutation rates or to balancing selection (in our case due to linkage of genes in evolutionary strata to mating-type genes), by comparing a model where all loci in the dataset evolve neutrally to an alternative model where *N* loci depart from neutrality (59, 60). Because MLHKA tests require a set of control loci that evolve neutrally, we applied these tests to pairwise comparisons between each stratum and the pseudo-autosomal region. To perform the MLHKA tests, we considered the pooled CDS sequences associated with the a_1 and a_2 mating-types for each stratum in each of *M. lychnidis-dioicae* and *M. silenes-dioicae* and used the genome of *M. violaceum sens. str.* as an outgroup. In order to improve divergence estimates, alignments were re-aligned with MACSE (61). Only synonymous sites were taken into account, and singletons were excluded. Unless stated otherwise, tests were run with 1,000,000 iterations of the Markov chain, and repeated at least three times with different random seed numbers to ensure convergence. We arbitrarily chose a starting value of 10 for divergence time, as this value is of little importance when the number of

iterations is high enough for the Markov chains to converge (58). Synonymous nucleotidic diversity (θ_π) was computed with EggLib version 2 (56) and used as starting value for theta. As the test assumes independence between loci, we concatenated the alignments of the CDS for each evolutionary stratum. For the largest stratum (the black stratum), we randomly sampled and concatenated CDS for 20 genes, as the high number of genes in this stratum resulted in unreasonable running times. For the two most recent strata (red and green strata), we also ran the tests without concatenating the alignments, with 2,000,000 million of iterations of the Markov chains. This yielded similar results as concatenating the CDS. *Microbotryum lychnidis-dioicae* displays a strong population structure in Europe (51, 62), which can lead to over-estimate the diversity in neutral loci and result in false negative tests. In fact, visual inspection of the alignments showed that most polymorphic sites in the PARs in this species corresponded to fixed differences between genetic clusters. We therefore also ran tests separately on the two genetic clusters for which we had several strains of each mating-type, i.e., the Southern and North-Western clusters (51). We corrected p-values for multiple testing within each species with a Benjamini and Hochberg correction (R function p.adjust). In *M. silenes-dioicae*, tests for all strata were significant (adjusted p-values < 0.05, Table S7A), indicating that balancing selection was more likely than elevated mutation rates for explaining the higher diversity in strata than in the PARs. In *M. lychnidis-dioicae*, tests were also significant for the purple, blue, black and orange strata (adjusted p-values < 0.05, Table S7B-D). The difference in diversity between the red stratum and the PAR was marginally significant when considering the whole data set, and significant when the tests were run separately on two genetic clusters (Table S7B-D). There was no significant difference in diversity between the green stratum and the PAR in *M. lychnidis-dioicae*, suggesting that suppressed recombination is not complete there in this species, or that it is too recent to have allowed an accumulation of differences between mating types.

SI References

1. Feldbrugge M, Kamper J, Steinberg G, & Kahmann R (2004) Regulation of mating and pathogenic development in *Ustilago maydis*. *Curr Op Microbiol* 7:666-672.
2. Kuees U (2015) From two to many: Multiple mating types in Basidiomycetes. *Fung Biol Rev* 29(3-4):126-166.
3. Casselton LA & Kues U (2007) The origin of multiple mating types in the model mushrooms *Coprinopsis cinerea* and *Schizophyllum commune*. *Sex in Fungi*, eds Heitman J, Kronstad J, Taylor J, & Casselton L (ASM Press, Washington, DC), Vol **88**, pp 142 - 147.
4. Kues U (2000) Life history and developmental processes in the basidiomycete *Coprinus cinereus*. *Microbiol Mol Biol Rev* 64(2):316-453.
5. James TY (2015) Why mushrooms have evolved to be so promiscuous: Insights from evolutionary and ecological patterns. *Fung Biol Rev* 29(3-4):167-178.
6. Nieuwenhuis BPS, *et al.* (2013) Evolution of uni- and bifactorial sexual compatibility systems in fungi. *Heredity* 111:445-455.
7. Giraud T, Yockteng R, Lopez-Villavicencio M, Refregier G, & Hood ME (2008) The mating system of the anther smut fungus, *Microbotryum violaceum*: selfing under heterothallism. *Euk Cell* 7:765-775.
8. Heitman J, Sun S, & James TY (2013) Evolution of fungal sexual reproduction. *Mycologia* 105(1):1-27.
9. Kües U, James T, & Heitman J (2011) The mycota XIV : Mating type in basidiomycetes: Unipolar, bipolar, and tetrapolar paterns of sexuality. *Evolution of fungi and fungal-like organisms*, eds Pöggeler S & Wöstemeyer J (Springer-Verlag, Berlin, Heidelberg Germany).
10. Bakkeren G & Kronstad JW (1994) Linkage of mating type loci distinguishes bipolar from tetrapolar mating in basidiomycetous smut fungi. *Proc Natl Acad Sci USA* 91:7085-7089.
11. Idnurm A, Hood ME, Johannesson H, & Giraud T (2015) Contrasted patterns in mating-type chromosomes in fungi: Hotspots versus coldspots of recombination. *Fung Biol Rev* 29(3-4):220-229.
12. Badouin H, *et al.* (2015) Chaos of rearrangements in the mating-type chromosomes of the anther-smut fungus *Microbotryum lychnidis-dioicae*. *Genetics* 200(4):1275-1284.
13. Fraser JA, *et al.* (2004) Convergent evolution of chromosomal sex-determining regions in the animal and fungal kingdoms. *PLoS Biol* 2:2243-2255.
14. Hood ME & Antonovics J (2000) Intratetrad mating, heterozygosity, and the maintenance of deleterious alleles in *Microbotryum violaceum (=Ustilago violacea)*. *Heredity* 85:231-241.
15. Menkis A, Jacobson DJ, Gustafsson T, & Johannesson H (2008) The mating-type chromosome in the filamentous ascomycete *Neurospora tetrasperma* represents a model for early evolution of sex chromosomes. *PLoS Genet* 4(3):e1000030.
16. Zakharov IA (1986) Some principles of the gene localization in eukaryotic chromosomes. Formation of the problem and analysis of nonrandom localization of the mating-type loci in some fungi. *Genetika* 22:2620-2624.
17. Zakharov IA (2005) Intratetrad mating and its genetic and evolutionary consequences. *Russ J Genet* 41:508-519.
18. Abbate JL & Hood ME (2010) Dynamic linkage relationships to the mating-type locus in automictic fungi of the genus *Microbotryum*. *J. Evol. Biol* 23(8):1800-1805.
19. Charlesworth D (2016) The status of supergenes in the 21st century: recombination suppression in Batesian mimicry and sex chromosomes and other complex adaptations. *Evol App* 9(1):74-90.

20. Antonovics J & Abrams JY (2004) Intratetrad mating and the evolution of linkage relationships. *Evolution* 58(4):702-709.

21. Johnson LJ, Antonovics J, & Hood ME (2005) The evolution of intratetrad mating rates. *Evolution* 59(12):2525-2532.

22. Ironside JE (2010) No amicable divorce? Challenging the notion that sexual antagonism drives sex chromosome evolution. *Bioessays* 32(8):718-726.

23. Kniep H (1919) Untersuchungen uber den Antherenbrand (*Ustilago violacea* Pers.). Ein Beitrag zum Sexualitatsproblem. *Z Bot* 11:257-284.

24. Hood ME (2002) Dimorphic mating-type chromosomes in the fungus *Microbotryum violaceum*. *Genetics* 160:457-461.

25. Hood ME, Antonovics J, & Koskella B (2004) Shared forces of sex chromosome evolution in haploids and diploids. *Genetics* 168:141-146.

26. Hood ME, Petit E, & Giraud T (2013) Extensive divergence between mating-type chromosomes of the anther-smut fungus. *Genetics* 193(1):309-315.

27. Fontanillas E, *et al.* (2015) Degeneration of the non-recombining regions in the mating type chromosomes of the anther smut fungi. *Mol Biol Evol* 32:928-943.

28. Votintseva AA & Filatov DA (2009) Evolutionary strata in a small mating-type-specific region of the smut fungus *Microbotryum violaceum*. *Genetics* 182(4):1391-1396.

29. Whittle CA, Votintseva A, Ridout K, & Filatov DA (2015) Recent and massive expansion of the mating-type specific region in the smut fungus *Microbotryum*. *Genetics* 199:809-816.

30. Menkis A, Whittle C, & Johannesson H (2010) Gene genealogies indicates abundant gene conversions and independent evolutionary histories of the mating-type chromosomes in the evolutionary history of *Neurospora tetrasperma*. *BMC Evol Biol* 10(1):234.

31. Sun S, Hsueh Y-P, & Heitman J (2012) Gene conversion occurs within the mating-type locus of *Cryptococcus neoformans* during sexual reproduction. *PLoS Genet* 8(7):e1002810.

32. Pandey RS & Azad RK (2016) Deciphering evolutionary strata on plant sex chromosomes and fungal mating-type chromosomes through compositional segmentation. *Plant Mol Biol* 90(4-5):359-373.

33. Hood ME & Antonovics JA (2004) Mating within the meiotic tetrad and the maintenance of genomic heterozygosity. *Genetics* 166:1751-1759.

34. Thomas A, Shykoff J, Jonot O, & Giraud T (2003) Sex-ratio bias in populations of the phytopathogenic fungus *Microbotryum violaceum* from several host species. *Int J Plant Sci* 164(4):641-647.

35. Hood ME, Scott M, & Hwang M (2015) Breaking linkage between mating compatibility factors: Tetrapolarity in *Microbotryum*. *Evolution* 69(10):2561-2572.

36. Koren S, *et al.* (2012) Hybrid error correction and de novo assembly of single-molecule sequencing reads. *Nat Biotechnol* 30:693-700.

37. Foissac S, *et al.* (2008) Genome annotation in plants and fungi: EuGène as amodel platform. *Current Bioinformatics* 3:87-97.

38. Consortium TU (2011) Ongoing and future developments at the Universal Protein Resource. *Nucleic Acids Res* 39:D214-D219.

39. Krzywinski MI, *et al.* (2009) Circos: An information aesthetic for comparative genomics. *Genom Res* 19:1639-1645.

40. Li L, Stoeckert CJ, & Roos D (2003) OrthoMCL: identification of ortholog groups for eukaryotic genomes. *Genome Research* 13:2178-2189.

41. van Dongen S (2000) Graph clustering by flow simulation. PhD (University of Utrecht, The Netherlands).

42. Edgar R (2004) MUSCLE: multiple sequence alignment with high accuracy and high throughput. *Nucleic Acids Res.* 32 1792-1797.

43. Abascal F, Zardoya R, & Telford M (2010) TranslatorX: multiple alignment of nucleotide sequences guided by amino acid translations. *Nucleic Acids Res* 38:W7-13.

44. Stamatakis A (2006) RAxML-VI-HPC: maximum likelihood-based phylogenetic analyses with thousands of taxa and mixed models. *Bioinformatics* 22:2688-2690.

45. Capella-Gutierrez S, Silla-Martinez JM, & Gabaldon T (2009) trimAl: a tool for automated alignment trimming in large-scale phylogenetic analyses. *Bioinformatics* 25:1972-1973.

46. Salichos L, Stamatakis A, & Rokas A (2014) Novel Information Theory-Based Measures for Quantifying Incongruence among Phylogenetic Trees. *Molyang Biol Evol* 31(5):1261-1271.

47. Bouckaert R, *et al.* (2014) BEAST 2: a software platform for Bayesian evolutionary analysis. *PLoS Comput Biol* 10:e1003537.

48. Gladieux P, *et al.* (2011) Maintenance of fungal pathogen species that are specialized to different hosts: allopatric divergence and introgression through secondary contact. *Mol Biol Evol* 28:459-471.

49. Smit A & Green P (RepeatMasker at http://www.repeatmasker.org/.

50. Jurka J (1998) Repeats in genomic DNA: mining and meaning. *Curr Opin Struct Biol* 8:333-337.

51. Badouin H, *et al.* (2017) Widespread selective sweeps throughout the genome of model plant pathogenic fungi and identification of effector candidates. *Mol Ecol* 26:2041-2062.

52. Oudemans P, *et al.* (1998) The distribution of mating type bias in natural populations of the anther smut *Ustilago violacea (=Microbotryum violaceum)* on *Silene alba (= S. latifolia)* in Virginia. *Mycologia* 90:372-381.

53. Luo R, *et al.* (2012) SOAPdenovo2: an empirically improved memory-efficient short-read de novo assembler. *GigaScience* 1(1):18.

54. Devier B, Aguileta G, Hood M, & Giraud T (2009) Ancient trans-specific polymorphism at pheromone receptor genes in basidiomycetes. *Genetics* 181:209–223.

55. Koboldt D, *et al.* (2012) VarScan 2: Somatic mutation and copy number alteration discovery in cancer by exome sequencing. *Genom Res* 22:568-576.

56. De Mita S & Siol M (2012) EggLib: processing, analysis and simulation tools for population genetics and genomics. *BMC Genetics* 13(1):27.

57. Huerta-Cepas J, Serra F, & Bork P (2016) ETE 3: Reconstruction, Analysis, and Visualization of Phylogenomic Data. *Mol Biol Evol* 33(6):1635-1638.

58. Wright SI & Charlesworth B (2004) The HKA test revisited: A maximum-likelihood-ratio test of the standard neutral model. *Genetics* 168(2):1071-1076.

59. Qiu S, Bergero R, & Charlesworth D (2013) Testing for the Footprint of Sexually Antagonistic Polymorphisms in the Pseudoautosomal Region of a Plant Sex Chromosome Pair. *Genetics* 194(3):663-+.

60. Wright SI, *et al.* (2006) Testing for effects of recombination rate on nucleotide diversity in natural populations of Arabidopsis lyrata. *Genetics* 174(3):1421-1430.

61. Ranwez V, Harispe S, Delsuc F, & Douzery E (2011) MACSE: Multiple alignment of coding sequences accounting for frameshifts and stop codons. *PLoS ONE* 6:e22594.

62. Vercken E, *et al.* (2010) Glacial refugia in pathogens: European genetic structure of anther smut pathogens on *Silene latifolia* and *S. dioica. PloS Path* 6:e1001229.

List of SI Figures

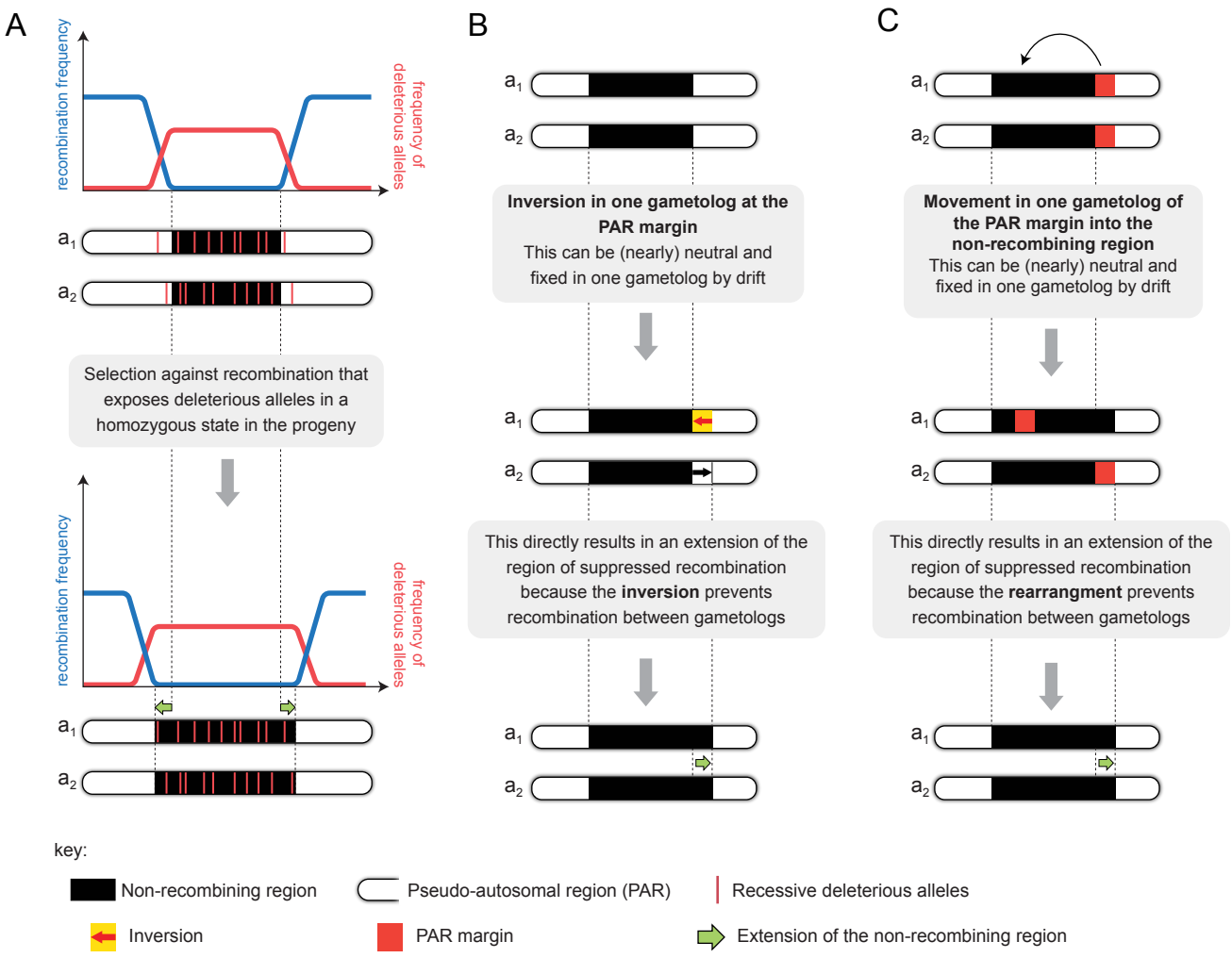

Fig. S1. **Hypotheses for the generation of evolutionary strata in sex or mating-type chromosomes. (A)** Expansion of linkage to the mating-type loci that encompasses partially linked genetic load loci, favoring permanent sheltering in a heterozygous state. This may occur if recombination frequency gradually decreases from the non-recombining region into the PAR, so that partial linkage (linkage disequilibrium) to mating-type or sex-determining genes makes selection against recessive deleterious alleles less efficient. This may allow deleterious alleles to increase in frequency in these PAR regions at the margin of the non-recombining region, further selecting for cessation of recombination. Rare recombination events would generate individuals homozygous for deleterious alleles and would therefore be selected against. Complete linkage of these PAR regions in linkage disequilibrium with mating type would be selected for. Alternative mechanisms for explaining suppressed recombination involve neutral inversions **(B)** or rearrangements **(C)** extending the region of suppressed recombination; these could be fixed by drift in one of the sex or mating-type chromosomes and arrest recombination between sex or mating-type chromosomes.

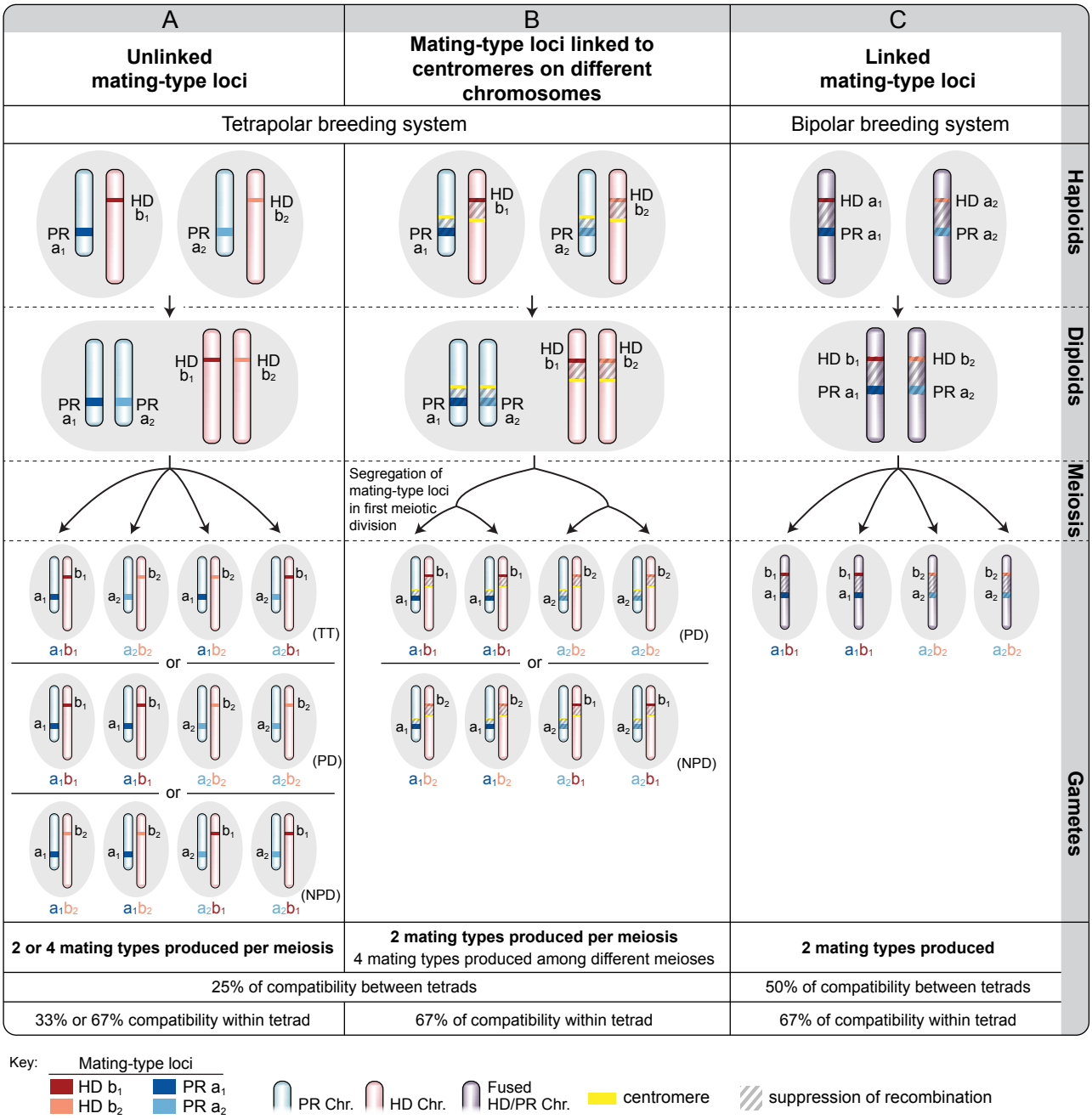

Fig. S2. Odds of compatibility among gametes of a diploid individual in basidiomycete fungi. Gametes are fully compatible only if they carry different alleles at both mating-type loci, i.e., the PR (including pheromone receptor and pheromone genes, with a_1 and a_2 alleles) and HD (including homeodomain genes, with b_1 and b_2 alleles) loci. (A) Under tetrapolarity with PR and HD mating-type loci unlinked from each other and from the centromeres (shown here located in different chromosomes, blue and red, respectively), the percentage of compatibility of a given gamete among the other gametes produced by the same diploid individual is 25% across multiple meioses (a given gamete is compatible with one of every four gametes), and the percentage is 33% within tetrad (a given gamete is compatible with one of the other three gametes in the tetrad) or 67% (a given gamete is compatible with two of the three remaining gametes in the tetrad) depending on segregation of the mating type alleles. The different types of gametes produced are tetratypes (TT), parental ditypes (PD) or non-parental ditypes (NPD), which depends on allele segregation and on whether a crossing-over occurred between one of the two loci and the centromere. (B) Under tetrapolarity with PR and HD mating-type genes linked to the centromeres of different chromosomes (blue and red, respectively), the percentage of compatibility of a given gamete among the other gametes produced by the same diploid individual is 25% across multiple meioses but 67% within a tetrad (a given gamete is compatible with two of the three other gametes in the tetrad) due to the segregation of the variation occurring only at meiosis I for both mating type loci. The different types of gametes produced are parental ditypes (PD) or non-parental ditypes (NPD), which depends on segregation. (C) Under bipolarity, i.e., with HD and PR loci fully linked to each other on the same chromosome, the percentage of compatibility of a given gamete among the other gametes produced by the same diploid individual is 50% across multiple meioses (a given gamete is compatible with two of every four gametes), and 67% within a single meiotic tetrad (a given gamete is compatible with two of the three other gametes in the tetrad).

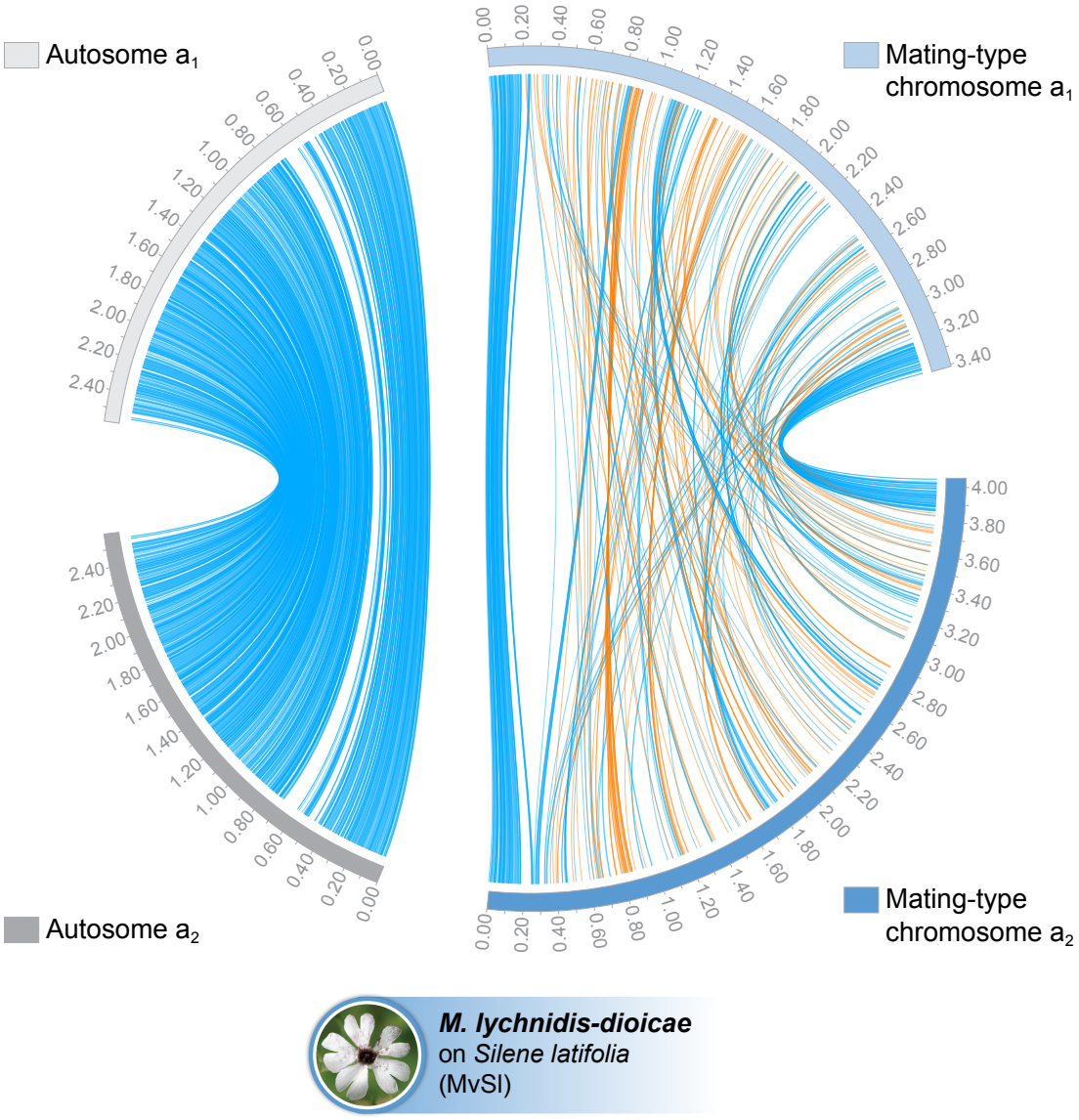

Fig. S3. **Comparison of gene order between *Microbotryum lychnidis-dioicae* chromosomes.** a_1 (top) and a_2 (bottom) mating chromosomes of *M. lychnidis-dioicae*; an autosome pair is shown at the left and the mating-type chromosomes at the right. Blue and orange lines link regions with collinearity across > 5 kb, with the orange links corresponding to inversions. The genomic regions without links correspond to highly rearranged regions. The recombining regions (the autosome and the pseudo-autosomal regions, PARs) are highly collinear between a_1 and a_2 chromosomes, despite a highly selfing mating system, while the non-recombining region on the mating-type chromosome is highly rearranged.

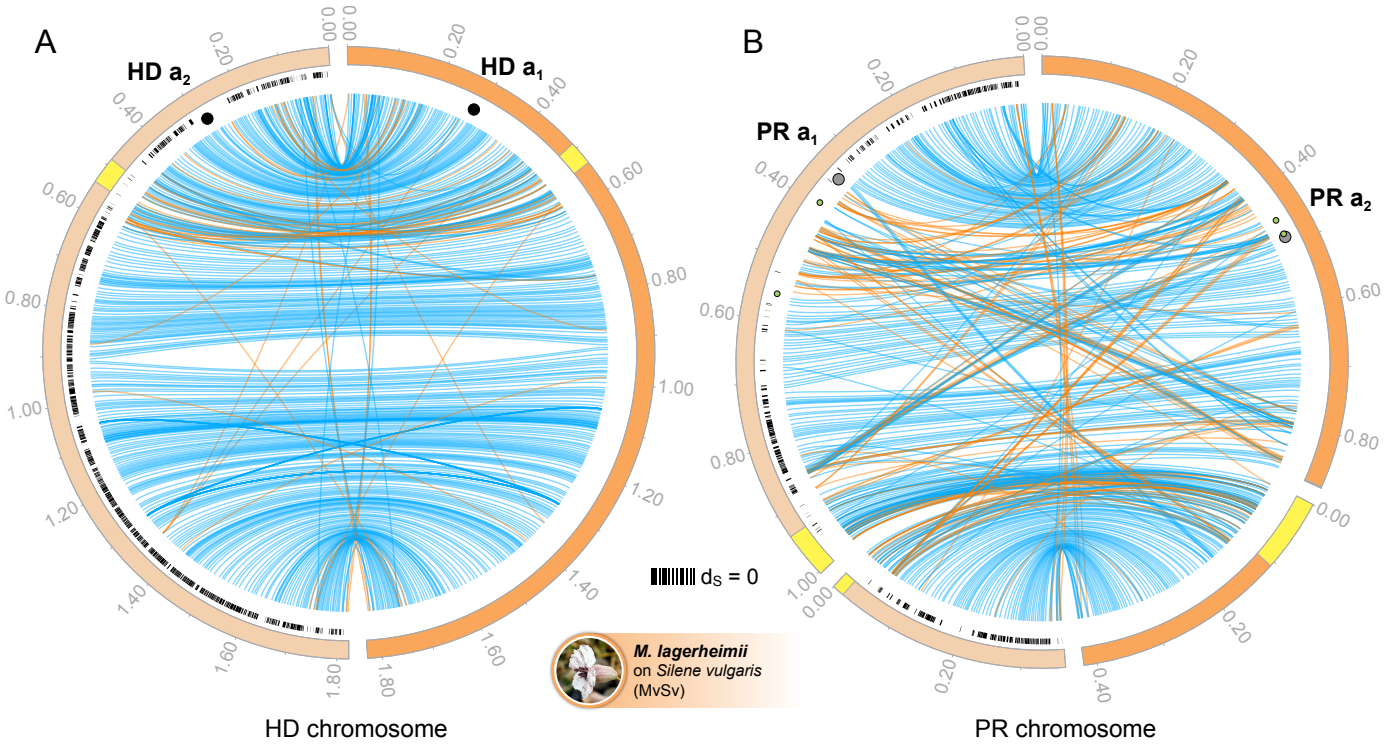

Fig. S4. **Synteny between a_1 and a_2 mating-type chromosomes of *Microbotryum lagerheimii*.** The homeodomain (HD) mating-type chromosomes are displayed in the left circle and the pheromone receptor (PR) mating-type chromosomes in the right circle. The HD genes are indicated by black circles, the pheromone receptor gene by grey circles and the two pheromone genes by small green circles. Blue and orange lines link regions with collinearity across > 1 kb, with the orange links corresponding to inversions. The genomic region between the pheromone receptor and pheromone genes in the a_1 mating-type chromosomes is rearranged compared to the a_2 mating-type chromosomes. Black marks along the contig circles indicate genes with no synonymous differentiation between a_1 and a_2 alleles within the sequenced individual (d_S = 0). Yellow regions on the outer track indicate centromere-specific repeats (12).

A

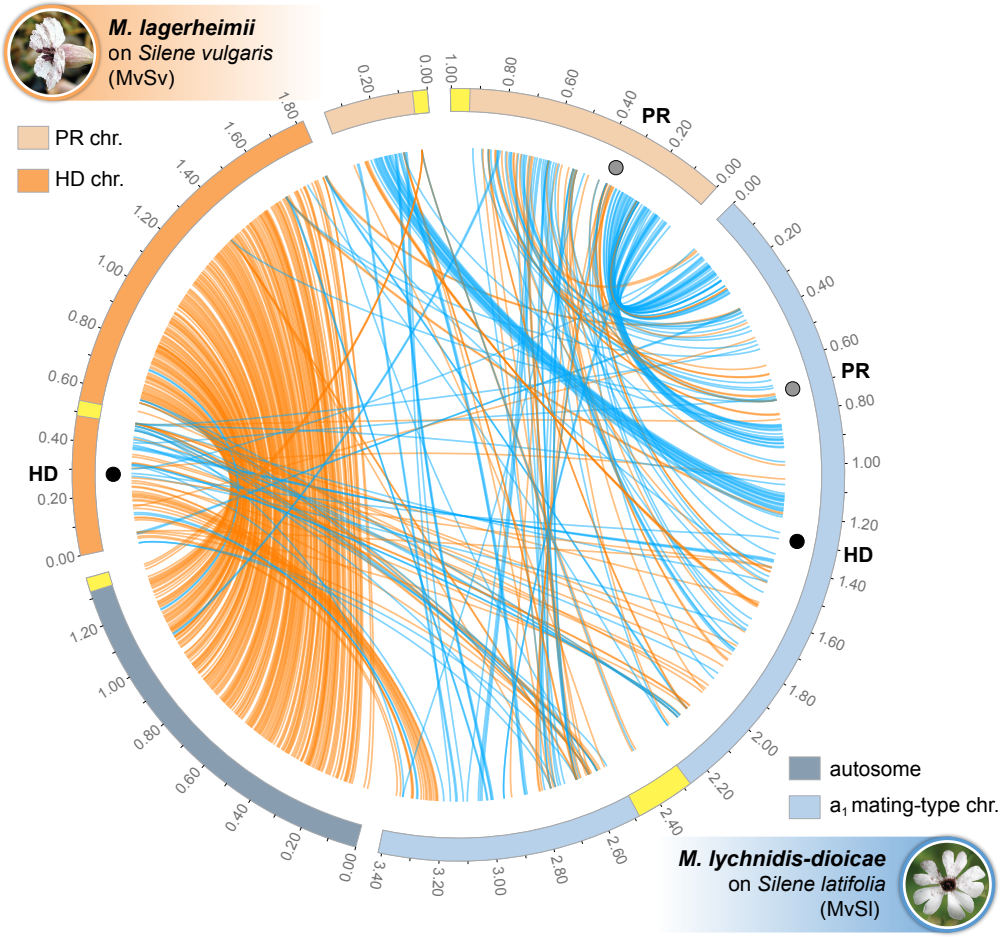

Fig. S5. Comparison of gene order between mating-type chromosomes. In all panels (A-E), the outer tracks illustrate assembled chromosomes/contigs and are color coded by species as in Fig. 1. The positions of HD and PR genes are indicated by the black and grey small circles, respectively. Yellow regions on the outer track indicate the centromere-specific repeats (12) and, when represented, red ("R") and green ("G") regions indicate the genomic location of the red and green genes as described in Fig. 4B. **(A)** Comparison between the a_1 mating-type chromosomes (chr.) of *Microbotryum lagerheimii* (orange contigs, with light orange for the PR mating-type chromosome and dark orange for the HD mating-type chromosome) and the mating-type chromosome of *M. lychnidis-dioicae* (light blue contig), as well as an autosomal contig of *M. lychnidis-dioicae* (dark blue contig). Blue and orange lines link regions with collinearity across > 2 kb, with orange corresponding to inversions. Genomic regions without links correspond to highly rearranged regions.

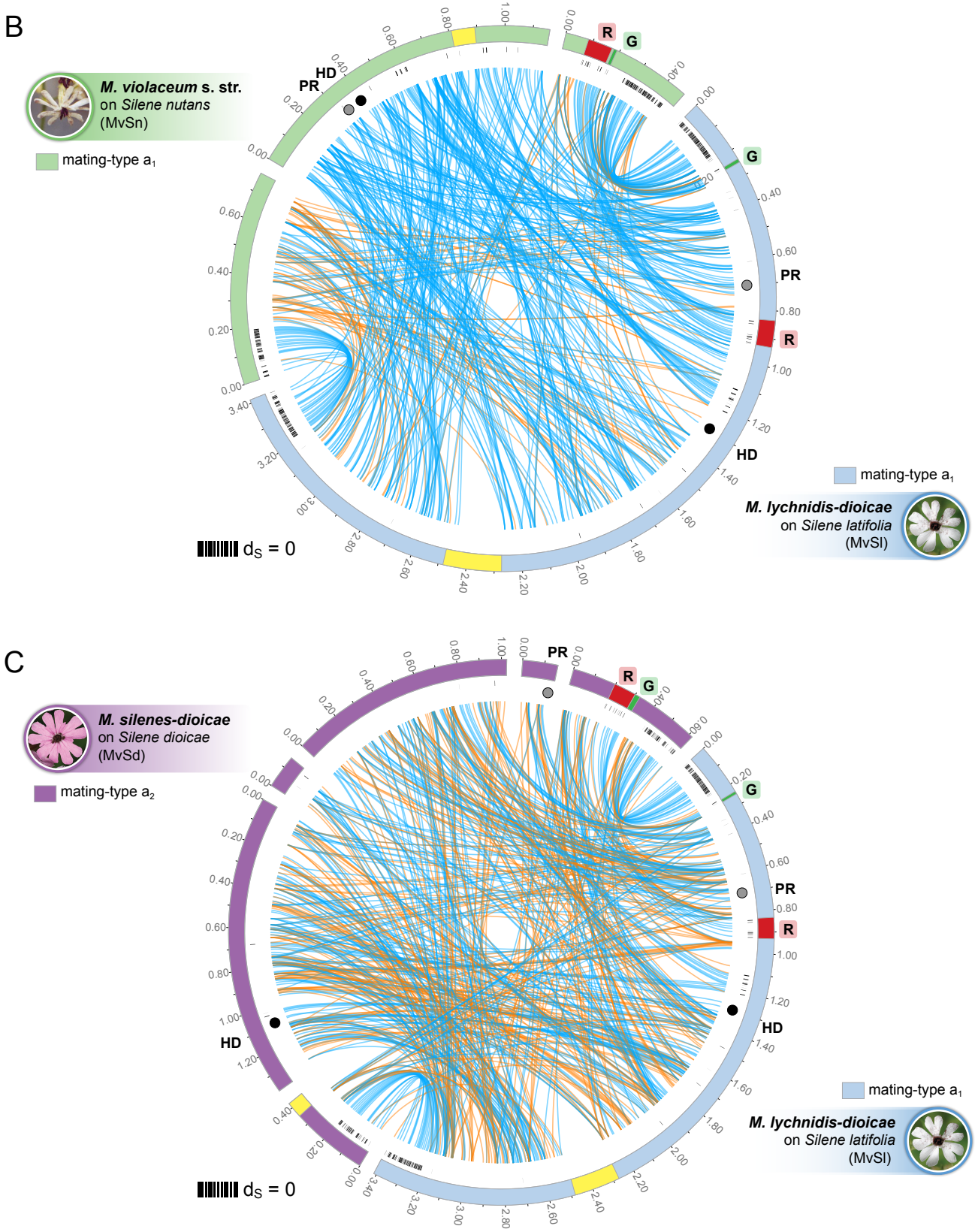

Fig. S5. Continued**. (B)** Comparison of a_1 mating-type chromosomes of *Microbotryum lychnidis-dioicae* (right, light blue contig) and *M. violaceum s. str.* (left, light green contigs). It should be noted that the orientation of the central contig in the a_1 *M. violaceum s. str.* mating-type chromosome could not be assessed, so all its links were drawn blue. The black marks along the contig circle indicate genes that have no synonymous substitution between a_1 and a_2 alleles ($d_S = 0$) in *M. lychnidis-dioicae*. **(C)** Comparison between the a_1 mating-type chromosomes of *M. silenes-dioicae* (dark purple contigs on the left) and *M. lychnidis-dioicae* (light blue contig on the right). Blue and orange lines link regions with collinearity across > 3 kb, with orange corresponding to inversions (note that the *M. silenes-dioicae* central contigs could not be ordered or oriented). All the remaining features are as described in panel (A).

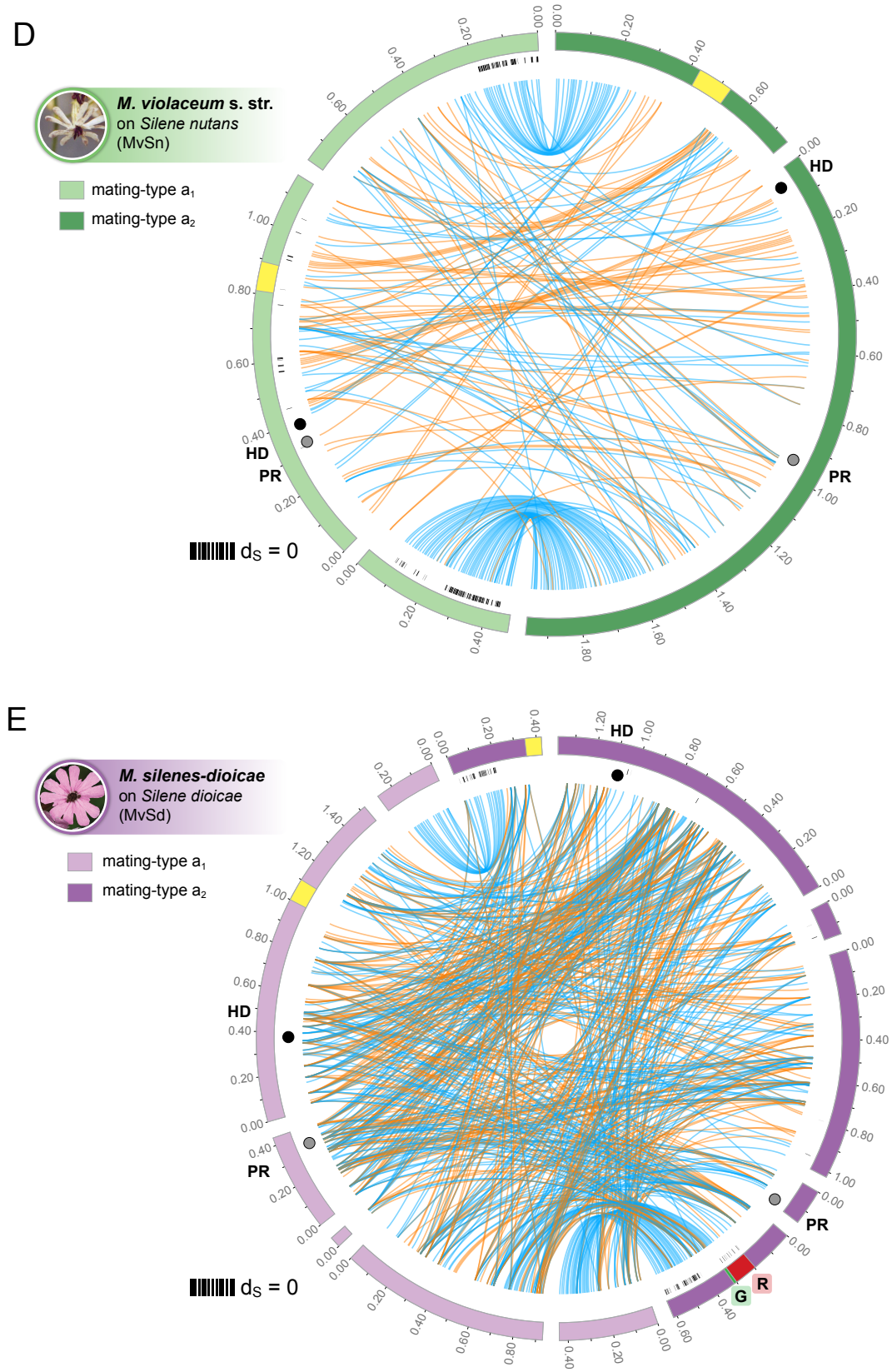

Fig. S5. Continued**. (D)** Comparison of a_1 (left, light green) and a_2 (right, dark green) mating-type chromosomes of *M. violaceum s. stricto*. Blue and orange lines link regions with collinearity across > 3 kb, with orange corresponding to inversions. It should be noted that the orientation of the central contig in the a_1 mating-type chromosome could not be assessed. The black marks along the contig circle indicate the genes with no synonymous substitutions between a_1 and a_2 alleles (d_S=0) in *M. violaceum s. stricto*. **(E)** Comparison of a_1 (left, light purple) and a_2 (right, dark purple) mating-type chromosomes of *M. silenes-dioicae*. Blue and orange lines link regions with collinearity across >3 kb, with orange corresponding to inversions. Note that the central contigs could not be ordered or oriented. The location of the red ("R") and green ("G") genes in Fig. 4B are indicated in the a_2 genome. The black marks along the contig circle indicate the genes with no synonymous substitutions between a_1 and a_2 alleles (d_S = 0). The remaining features are as described in panel (A).

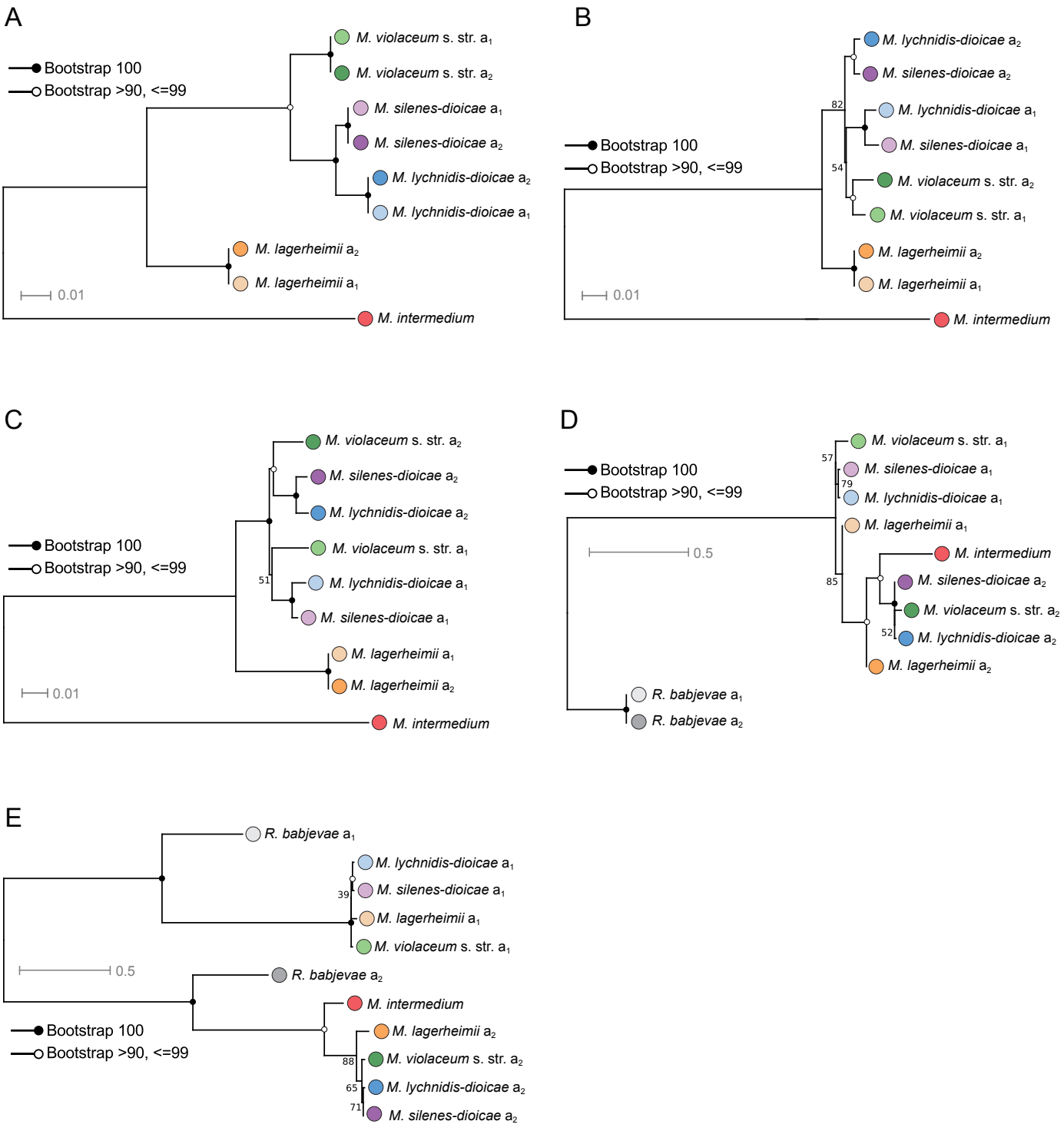

Fig. S6. Examples of gene genealogies at non-mating type genes showing different levels of trans-specific polymorphism, i.e., with more or less ancient linkage to mating type. Bootstraps are shown at nodes and the branch length scale is indicated. Strains of the same species are indicated by circles of the same color (a_1, lighter variant; a_2, darker variant) and according to Fig. 1. **(A)** No trans-specific polymorphism (orthogroup belonging to the *M. lychnidis-dioicae* PAR). **(B)** Trans-specific polymorphism across *M. lychnidis-dioicae* and *M. silenes-dioicae* (orthogroup belonging to the *M. lychnidis-dioicae* black stratum). **(C)** Trans-specific polymorphism across *M. lychnidis-dioicae, M. silenes-dioicae* and *M. violaceum* s. str. (orthogroup belonging to the *M. lychnidis-dioicae* black stratum). **(D)** Trans-specific polymorphism across *M. lychnidis-dioicae, M. silenes-dioicae, M. violaceum s. str.* and *M. lagerheimii* (orthogroup belonging to the *M. lychnidis-dioicae* PR stratum). **(E)** Trans-specific polymorphism across *M. lychnidis-dioicae, M. silenes-dioicae, M. violaceum s. str. M. lagerheimii* and *Rhodotorula babjevae* (orthogroup belonging to the *M. lychnidis-dioicae* orange stratum).

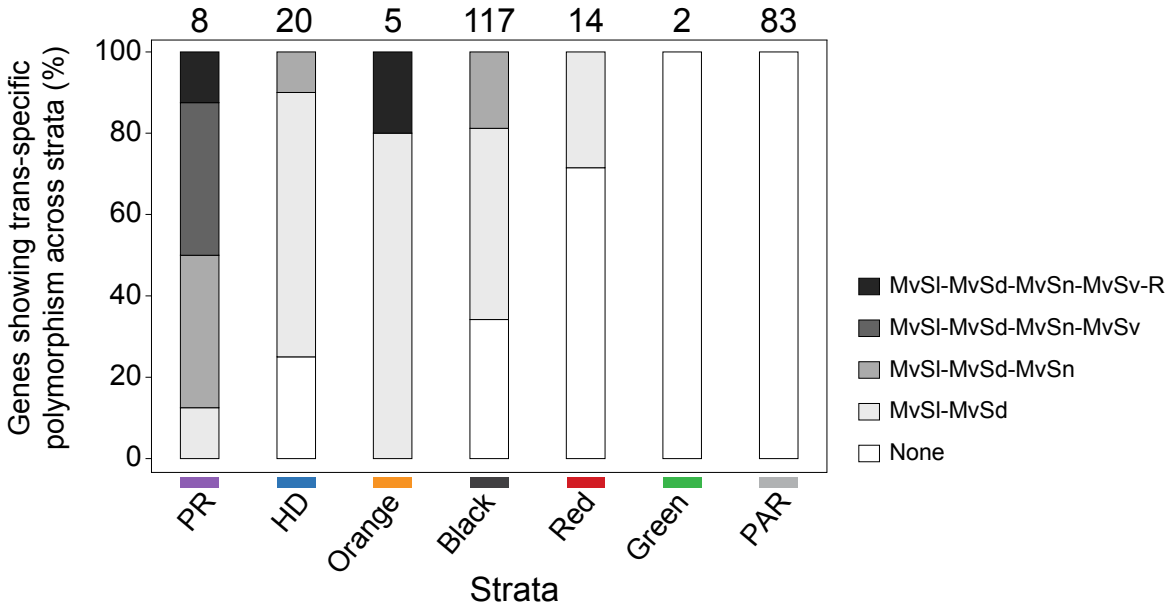

Fig. S7. **Cumulative percentage of genes showing trans-specific polymorphism across strata and age of trans-specific polymorphism relative to speciation events.** Black - single-copy genes with deep trans-specific polymorphism including all species, *M. lychnidis-dioicae* (MvSl), *M. silenes-dioicae* (MvSd), *M. violaceum* s. str. (MvSn), *M. lagerheimii* (MvSv), and even *Rhodotorula babjevae* (R); dark grey - genes showing trans-specific polymorphism including only *M. lychnidis-dioicae, M. silenes-dioicae, M. violaceum* s. str., and *M. lagerheimii*; grey - genes showing trans-specific polymorphism with only *M. lychnidis-dioicae, M. silenes-dioicae* and *M. violaceum s. str.;* light grey - genes with trans-specific polymorphism only between *M. lychnidis-dioicae* and *M. silenes-dioicae*; white - genes with no trans-specific polymorphism. Numbers on the top indicate genes for which gene genealogies with all species and alleles were computed. See Figure S6 for examples of gene genealogies with different levels of trans-specific polymorphism.

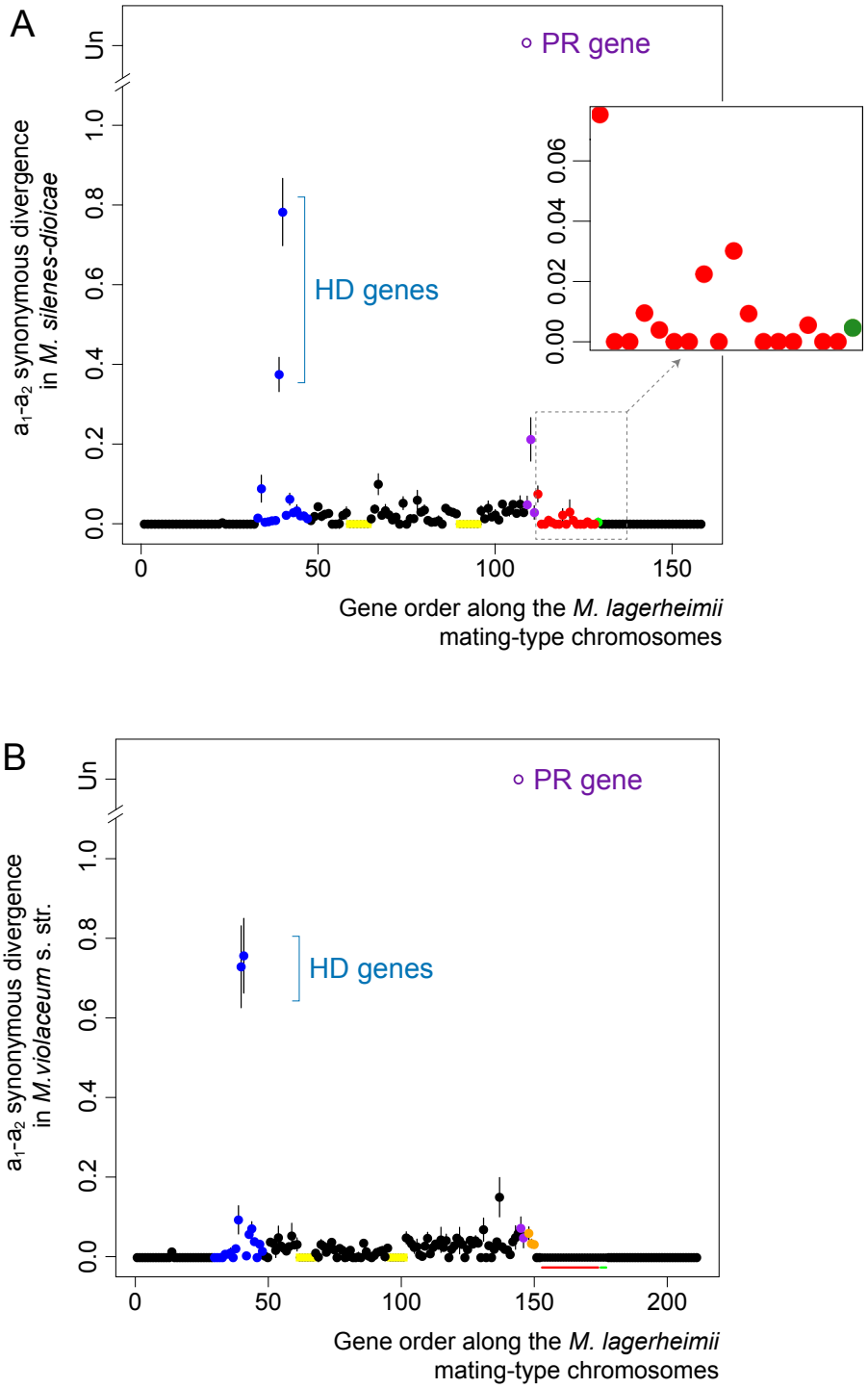

Fig. S8. Synonymous divergence between alleles associated with a_1 and a_2 mating types in the sequenced diploid individual in each of *Microbotryum silenes-dioicae* and *M. violaceum s. stricto,* plotted along the ancestral gene order. Synonymous divergence between a_1-a_2 in *M. silenes-dioicae* **(A)** and *M. violaceum s. str.* **(B)** plotted in the ancestral genomic coordinates, as inferred from the *M. lagerheimii* a_1 mating-type chromosome. In both panels, points are mean d_S values per gene and error bars the standard errors. All non-transposable element genes shared by the mating-type chromosomes are depicted. Divergence between the a_1 and a_2 pheromone receptor (PR) was too extensive (54) and could not be computed in both species (it is plotted as an "unalignable" open circle to ease visualization of the various strata). The positions of the inferred ancestral centromeres are indicated by yellow boxes. Genes with non-zero d_S around the PR and HD mating-type loci within the sequenced individual of *M. lagerheimii* are colored in purple and blue, respectively. More recent putative evolutionary strata in *M. silenes-dioicae* (panel A) are indicated in red and green, and zoomed in on the inset shown on the upper right. In panel (B), the genes belonging to more recent evolutionary strata in *M. silenes-dioicae* and *M. lychnidis-dioicae* are indicated by red and green bars.

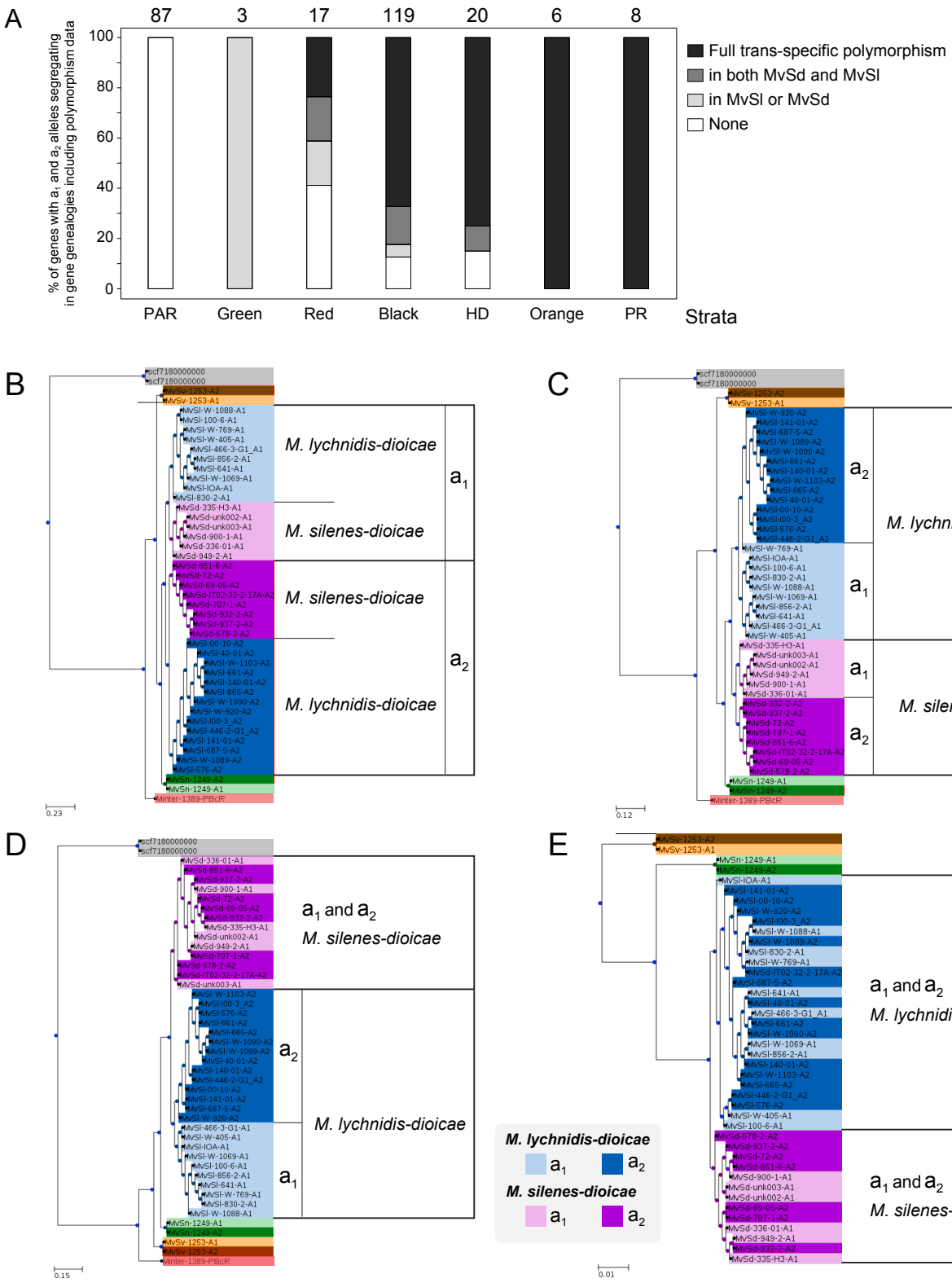

Fig. S9. Patterns of segregation of alleles at non-mating-type genes, associated with the a_1 and a_2 mating types, respectively, in gene genealogies using multiple resequenced genomes of *M. silenes-dioicae* (MvSd) and *M. lychnidis-dioicae* (MvSl). (A) Percentage (%) of gene genealogies showing different levels of segregation of a_1 and a_2 alleles: white - gene genealogies with mixed a_1 and a_2 *M. silenes-dioicae* and *M. lychnidis-dioicae* alleles; light grey - gene genealogies with a_1 and a_2 alleles separated in *M. silenes-dioicae* or *M. lychnidis-dioicae*, but not in both species; dark grey - gene genealogies with a_1 and a_2 alleles separated in both *M. silenes-dioicae* or *M. lychnidis-dioicae*, but without trans-specific polymorphism across the two species; black - gene genealogies with full trans-specific polymorphism. The numbers at the top indicate the number of genes for which information was available. **(B-E)** Examples of gene genealogies showing different levels of segregation of alleles at non-mating-type genes, associated with the a_1 and a_2 mating types, respectively (shown in lighter and darker color variants, respectively) based on the analyses of multiple *M. silenes-dioicae* (MvSd, purple) and *M. lychnidis-dioicae* (MvSl, blue) genomes. Alleles of *M. lagerheimii* (MvSv, orange), *M. violaceum s. str.* (MvSn, green), *M. intermedium* (Minter, red) and *Rhodotorula babjevae* (sfc, gray) are also included; **(B)** gene genealogy with full trans-specific polymorphism (red statum); **(C)** alleles at non-mating-type genes, associated with the a_1 and a_2 mating types, respectively, separated in both *M. silenes-dioicae* and *M. lychnidis-dioicae*, but without trans-specific polymorphism across the two species (red stratum); **(D)** gene genealogy with alleles at non-mating-type genes, associated with the a_1 and a_2 mating types, respectively, separated in *M. lychnidis-dioicae* only (red stratum); **(E)** intermingled alleles at non-mating-type genes, associated with the a_1 and a_2 mating types, respectively, of both *M. silenes-dioicae* and *M. lychnidis-dioicae* (pseudo-autosomal region, PAR).

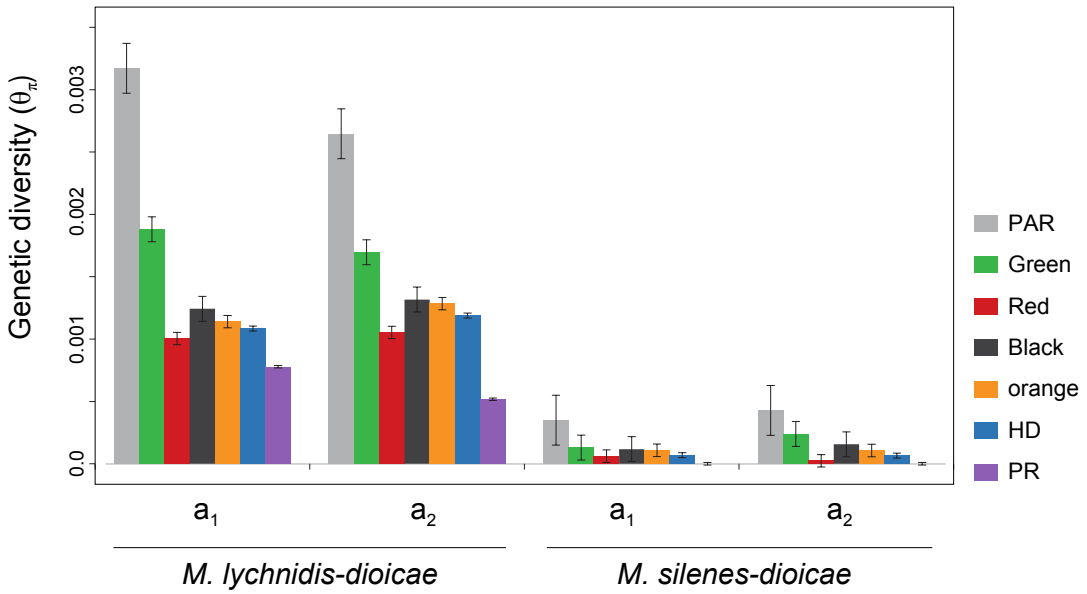

Fig. S10. *Microbotryum lychnidis-dioicae* and *M. silenes-dioicae* genetic diversity ($\theta\pi$) based on multiple genomes. Diversity (±SE) was estimated in a_1 or a_2 mating type separately, in the pseudo-autosomal regions (PARs) and the different evolutionary strata (green, red, black, orange, HD-proximal and PR-proximal). *M. silenes-dioicae* is known to display lower genetic diversity than *M. lychnidis-dioicae* (48, 51, 62).

List of SI Tables

Table S1. Synonymous substitution (d_S) means within diploid individuals between alleles associated to the a1 and a2 mating types for genes in the different putative strata and the pseudo-autosomal regions (PARs), number of genes and estimated dates for recombination suppression. Mean d_S and standard error (SE) across genes between the large putative strata, numbered in their presumed order of origin of suppressed recombination, whether they involve mating-type genes, the *Microbotryum* species in which recombination is suppressed in these strata, the estimated date of recombination suppression in strata where inference was possible, and number of genes ancestrally in *M. lychnidis-dioicae* in the strata (many genes have been lost from one or the other mating types following recombination suppression).

Stratum order	Stratum	Mean d_S ± SE	Involving mating-type genes?	Species in which recombination is suppressed	Estimated date recombination suppression	Number of genes ancestrally in *M. lychnidis-dioicae*
1	PR mating-type gene	Not alignable	Yes	All species	370 MYA (54)	3
2	HD mating-type genes	0.62 ± 0.326	Yes	All species		2
3	PR-proximal genes (purple)	0.112 ± 0.040	No	All species	2.1 MYA	31
4	HD-proximal genes (blue)	0.103 ± 0.045	No	All species		14
5	Black (linking PR and HD mating-type loci)	0.032 ± 0.002	Yes	*M. lychnidis-dioicae, M. silenes-dioicae* and *M. violaceum s. str.*	1.3 MYA	85
6	Orange	0.052 ± 0.015	No	*M. lychnidis-dioicae, M. silenes-dioicae* and *M. violaceum s. str.*		*7*
7	Red	0.018 ± 0.049	No	*M. lychnidis-dioicae* and *M. silenes-dioicae*	0.9 MYA	22
8	Green	0.004 ± 0.003	No	*M. lychnidis-dioicae* and *M. silenes-dioicae*		3
	pPAR (from the ancestral HD chromosome)	<0.0001	No	None		73
	qPAR (from the ancestral PR chromosome)	<0.0001	No	None		80

Table S2. Synonymous substitution (d_S) between alleles associated with the a_1 and a_2 mating types in three individuals of outgroup species for the genes belonging to the *Microbotryum lagerheimii* purple and blue strata. (A) *Sporobolomyces salmonicolor* (Ss) strains CBS 6832 vs. ML 2241; (B) *Rhodotorula toruloides* (Rt) strains JCM 10020 (A1B1) vs. JCM 10021 (A2B11); (C) *Leucosporidium scottii* (Ls) strains CBS 5930 vs. CBS 5931. The ID of the query gene from the reference *M. lychnidis-dioicae* genome, the ID in the outgroup genome, the d_S value and the putative function inferred from similarity are given. The only functions associated with mating or mating-type functions are the mating-type genes (highlighted in bold). The pheromone receptor genes are not shown as they could not be aligned between mating types.

(A)

MvSI-Query ID	Paired ID in the outgroup	d_S	Functional annotation
MvSI-1064-A1-R4_A1g00025	Ss_CBS6832|g3490.t1;Ss_ML2241|g967.t1	0.0253	glycoside hydrolase family 28 protein
MvSI-1064-A1-R4_A1g00175	Ss_CBS6832|g4453.t1;Ss_ML2241|g4966.t1	0.0177	ABC1-A atypical protein kinase
MvSI-1064-A1-R4_A1g00230	Ss_CBS6832|g4436.t1;Ss_ML2241|g4982.t1	0.0045	ASF1-like histone chaperone
MvSI-1064-A1-R4_A1g00478	Ss_CBS6832|g2690.t1;Ss_ML2241|g5108.t1	0.0167	protein disulfide-isomerase
MvSI-1064-A1-R4_A1g00495	Ss_CBS6832|g6519.t1;Ss_ML2241|g6611.t1	0.0232	nucleotide-binding protein/RRM_SF
MvSI-1064-A1-R4_A1g00591	**Ss_CBS6832|g5519.t1;Ss_ML2241|g1781.t1**	**0.3037**	**homeodomain transcription factor HD1**
MvSI-1064-A1-R4_A1g00592	**Ss_CBS6832|g5518.t1;Ss_ML2241|g1780.t1**	**0.3041**	**homeodomain transcription factor HD2**
MvSI-1064-A1-R4_A1g00593	Ss_CBS6832|g2692.t1;Ss_ML2241|g5106.t1	0.0223	5'-3' exoribonuclease 2
MvSI-1064-A1-R4_A1g00659	Ss_CBS6832|g307.t1;Ss_ML2241|g1640.t1	0.0285	alpha-mannosyltransferase, glycosyltransferase family 71 protein
MvSI-1064-A1-R4_A1g00726	Ss_CBS6832|g4454.t1;Ss_ML2241|g4962.t1	0.0173	defective in Cullin neddylation protein 1/UBA_like_SF
MvSI-1064-A1-R4_A1g00772	Ss_CBS6832|g2693.t1;Ss_ML2241|g5105.t1	0.0260	U3 snoRNP-associated protein Esf2 / RRM_ABT1_like
MvSI-1064-A1-R4_A1g00800	Ss_CBS6832|g2586.t1|corr;Ss_ML2241|g6295.t1|corr	0.0368	S-(hydroxymethyl)glutathione dehydrogenase / alcohol dehydrogenase
MvSI-1064-A1-R4_A1g00801	Ss_CBS6832|g6218.t1;Ss_ML2241|g6054.t1	0.0308	exosome complex protein LRP1
MvSI-1064-A1-R4_A1g00844	Ss_CBS6832|g3596.t1;Ss_ML2241|g741.t1	0.0609	hypothetical protein
MvSI-1064-A1-R4_A1g00854	Ss_CBS6832|g4447.t1;Ss_ML2241|g4977.t1	0.0555	karyopherin kap95
MvSI-1064-A1-R4_A1g00970	Ss_CBS6832|g2670.t1;Ss_ML2241|g3808.t1	0.0287	T-complex protein 1 subunit beta
MvSI-1064-A1-R4_A1g00971	Ss_CBS6832|g2640.t1;Ss_ML2241|g6034.t1	0.0593	dolichyldiphosphatase / PAP2_like
MvSI-1064-A1-R4_A1g00972	Ss_CBS6832|g2641.t1;Ss_ML2241|g6035.t1	0.0449	hypothetical protein
MvSI-1064-A1-R4_A1g00997	Ss_CBS6832|g3124.t1;Ss_ML2241|g781.t1	0.0024	hypothetical protein
MvSI-1064-A1-R4_A1g00998	Ss_CBS6832|g2641.t1|corr;Ss_ML2241|g6036.t1|corr	0.0293	U3 small nucleolar ribonucleoprotein IMP3 / Ribosomal protein S4/S9
MvSI-1064-A1-R4_A1g01017	Ss_CBS6832|g4458.t1;Ss_ML2241|g4960.t1	0.0349	phosphatidylethanolamine N-methyltransferase (PEMT)
MvSI-1064-A1-R4_A1g01154	Ss_CBS6832|g2758.t1;Ss_ML2241|g2001.t1	0.0684	ribosomal protein L1
MvSI-1064-A1-R4_A1g01159	Ss_CBS6832|g5531.t1;Ss_ML2241|g1794.t1	0.0478	bZIP transcription factor (AP-1)
MvSI-1064-A1-R4_A1g01160	Ss_CBS6832|g2542.t1;Ss_ML2241|g1752.t1	0.0300	COP9 signalosome complex subunit 2
MvSI-1064-A1-R4_A1g01161	Ss_CBS6832|g2659.t1;Ss_ML2241|g3820.t1	0.0212	mitochondrial carrier protein
MvSI-1064-A1-R4_A1g01162	Ss_CBS6832|g5512.t1;Ss_ML2241|g1774.t1	0.0186	hypothetical protein
MvSI-1064-A1-R4_A1g01163	Ss_CBS6832|g2660.t1;Ss_ML2241|g3819.t1	0.0627	ADP-ribosylation factor-like protein 2
MvSI-1064-A1-R4_A1g01388	Ss_CBS6832|g1143.t1;Ss_ML2241|g6591.t1	0.0183	ribosome assembly protein Noc2
MvSI-1064-A1-R4_A1g01440	Ss_CBS6832|g2708.t1;Ss_ML2241|g5917.t1	0.0458	autophagy-related protein 7 / E1-like protein-activating enzyme Gsa7p/Apg7p
MvSI-1064-A1-R4_A1g01441	Ss_CBS6832|g2773.t1;Ss_ML2241|g1987.t1	0.0234	zinc finger, C3HC4 RING-type protein
MvSI-1064-A1-R4_A1g01457	Ss_CBS6832|g2652.t1;Ss_ML2241|g3827.t1	0.0269	unnamed protein product
MvSI-1064-A1-R4_A1g01458	Ss_CBS6832|g2652.t1;Ss_ML2241|g3827.t1	0.0269	DNA-directed RNA polymerase III subunit RPC1

Table S2. Continued.

(B)

MvSI-Query ID	Paired ID in the outgroup	dS	Functional annotation
MvSI-1064-A1-R4_A1g00175	Rt_JCM10020_06889-R1;Rt_JCM10021_05528-R1	0.338	ABC1-A atypical protein kinase
MvSI-1064-A1-R4_A1g00230	Rt_JCM10020_06874-R1;Rt_JCM10021_05544-R1	0.382	ASF1-like histone chaperone
MvSI-1064-A1-R4_A1g00478	Rt_JCM10020_01934-R1;Rt_JCM10021_07790-R1	0.618	protein disulfide-isomerase
MvSI-1064-A1-R4_A1g00495	Rt_JCM10020_01942-R1;Rt_JCM10021_02138-R1	0.363	nucleotide-binding protein/RRM_SF
MvSI-1064-A1-R4_A1g00591	**Rt_JCM10020_02036-R1;Rt_JCM10021_02036-R1**	**0.692**	**homeodomain transcription factor HD1**
MvSI-1064-A1-R4_A1g00592	**Rt_JCM10020_02035-R1;Rt_JCM10021_02037-R1**	**0.648**	**homeodomain transcription factor HD2**
MvSI-1064-A1-R4_A1g00593	Rt_JCM10020_01962-R1;Rt_JCM10021_02108-R1	0.423	5'-3' exoribonuclease 2
MvSI-1064-A1-R4_A1g00659	Rt_JCM10020_01652-R1;Rt_JCM10021_00547-R1	0.357	alpha-mannosyltransferase, glycosyltransferase family 71 protein
MvSI-1064-A1-R4_A1g00726	Rt_JCM10020_06891-R1;Rt_JCM10021_05538-R1	0.210	defective in Cullin neddylation protein 1/UBA_like_SF
MvSI-1064-A1-R4_A1g00772	Rt_JCM10020_01963-R1;Rt_JCM10021_02107-R1	0.554	U3 snoRNP-associated protein Esf2 / RRM_ABT1_like
MvSI-1064-A1-R4_A1g00800	Rt_JCM10020_02223-R1;Rt_JCM10021_01846-R1	0.361	S-(hydroxymethyl)glutathione dehydrogenase / alcohol dehydrogenase
MvSI-1064-A1-R4_A1g00801	Rt_JCM10020_01998-R1;Rt_JCM10021_02076-R1	0.334	exosome complex protein LRP1
MvSI-1064-A1-R4_A1g00854	Rt_JCM10020_06883-R1;Rt_JCM10021_05536-R1	0.195	karyopherin kap95
MvSI-1064-A1-R4_A1g00970	Rt_JCM10020_02405-R1;Rt_JCM10021_03563-R1	0.472	T-complex protein 1 subunit beta
MvSI-1064-A1-R4_A1g00971	Rt_JCM10020_02275-R1;Rt_JCM10021_01791-R1	0.442	dolichyldiphosphatase / PAP2_like
MvSI-1064-A1-R4_A1g00972	Rt_JCM10020_02276-R1;Rt_JCM10021_01790-R1	0.367	hypothetical protein
MvSI-1064-A1-R4_A1g00997	Rt_JCM10020_04030-R1;Rt_JCM10021_02518-R1	0.423	hypothetical protein
MvSI-1064-A1-R4_A1g00998	Rt_JCM10020_02282-R1;Rt_JCM10021_01784-R1	0.496	U3 small nucleolar ribonucleoprotein IMP3 / Ribosomal protein S4/S9
MvSI-1064-A1-R4_A1g01017	Rt_JCM10020_06899-R1;Rt_JCM10021_05518-R1	0.523	phosphatidylethanolamine N-methyltransferase (PEMT)
MvSI-1064-A1-R4_A1g01154	Rt_JCM10020_02129-R1;Rt_JCM10021_01938-R1	0.223	ribosomal protein L1
MvSI-1064-A1-R4_A1g01159	Rt_JCM10020_02186-R1;Rt_JCM10021_01883-R1	0.270	bZIP transcription factor (AP-1)
MvSI-1064-A1-R4_A1g01160	Rt_JCM10020_02367-R1;Rt_JCM10021_03528-R1	0.537	COP9 signalosome complex subunit 2
MvSI-1064-A1-R4_A1g01161	Rt_JCM10020_02382-R1;Rt_JCM10021_03542-R1	0.334	mitochondrial carrier protein
MvSI-1064-A1-R4_A1g01162	Rt_JCM10020_02317-R1;Rt_JCM10021_01748-R1	0.370	hypothetical protein
MvSI-1064-A1-R4_A1g01163	Rt_JCM10020_02358-R1;Rt_JCM10021_01709-R1	0.425	ADP-ribosylation factor-like protein 2
MvSI-1064-A1-R4_A1g01388	Rt_JCM10020_04617-R1;Rt_JCM10021_04683-R1	0.394	ribosome assembly protein Noc2
MvSI-1064-A1-R4_A1g01440	Rt_JCM10020_05792-R1;Rt_JCM10021_07432-R1	0.565	autophagy-related protein 7 / E1-like protein-activating enzyme Gsa7p/Apg7p
MvSI-1064-A1-R4_A1g01441	Rt_JCM10020_02100-R1;Rt_JCM10021_01969-R1	0.380	zinc finger, C3HC4 RING-type protein
MvSI-1064-A1-R4_A1g01458	Rt_JCM10020_02343-R1;Rt_JCM10021_01724-R1	0.559	DNA-directed RNA polymerase III subunit RPC1

Table S2. Continued.

(C)

MvSI-Query ID	Paired ID in the outgroup	dS	Functional annotation
MvSI-1064-A1-R4_A1g00025	Ls_CBS5930|g7897.t1;Ls_CBS5931|g4047.t1	0.0000	glycoside hydrolase family 28 protein
MvSI-1064-A1-R4_A1g00175	Ls_CBS5930|g8243.t1;Ls_CBS5931|g3668.t1	0.0205	ABC1-A atypical protein kinase
MvSI-1064-A1-R4_A1g00230	Ls_CBS5930|g8248.t1;Ls_CBS5931|g3672.t1	0.1701	ASF1-like histone chaperone
MvSI-1064-A1-R4_A1g00478	Ls_CBS5930|g3772.t1|corr;Ls_CBS5931|g4597.t1|corr	0.0000	protein disulfide-isomerase
MvSI-1064-A1-R4_A1g00495	Ls_CBS5930|g3767.t1;Ls_CBS5931|g4602.t1	0.0000	nucleotide-binding protein/RRM_SF
MvSI-1064-A1-R4_A1g00591	**Ls_CBS5930|g2009.t1;Ls_CBS5931|g4188.t1**	**0.5762**	**homeodomain transcription factor HD1**
MvSI-1064-A1-R4_A1g00592	**Ls_CBS5930|g2008.t1;Ls_CBS5931|g4189.t1**	**0.5376**	**homeodomain transcription factor HD2**
MvSI-1064-A1-R4_A1g00593	Ls_CBS5930|g3769.t1;Ls_CBS5931|g4600.t1	0.0000	5'-3' exoribonuclease 2
MvSI-1064-A1-R4_A1g00659	Ls_CBS5930|g5144.t1;Ls_CBS5931|g1185.t1	0.0117	alpha-mannosyltransferase, glycosyltransferase family 71 protein
MvSI-1064-A1-R4_A1g00726	Ls_CBS5930|g3411.t1;Ls_CBS5931|g3664.t1	0.0155	defective in Cullin neddylation protein 1/UBA_like_SF
MvSI-1064-A1-R4_A1g00772	Ls_CBS5930|g3768.t1;Ls_CBS5931|g4601.t1	0.0000	U3 snoRNP-associated protein Esf2 / RRM_ABT1_like
MvSI-1064-A1-R4_A1g00800	Ls_CBS5930|g1990.t1|corr;Ls_CBS5931|g4209.t1|corr	0.0000	S-(hydroxymethyl)glutathione dehydrogenase / alcohol dehydrogenase
MvSI-1064-A1-R4_A1g00844	Ls_CBS5930|g3965.t1;Ls_CBS5931|g6949.t1	0.0058	hypothetical protein
MvSI-1064-A1-R4_A1g00854	Ls_CBS5930|g8369.t1|corr;Ls_CBS5931|g3662.t1	0.0159	karyopherin kap95
MvSI-1064-A1-R4_A1g00970	Ls_CBS5930|g6624.t1|corr;Ls_CBS5931|g3773.t1|corr	0.0000	T-complex protein 1 subunit beta
MvSI-1064-A1-R4_A1g00971	Ls_CBS5930|g5099.t1;Ls_CBS5931|g239.t1	0.0488	dolichyldiphosphatase / PAP2_like
MvSI-1064-A1-R4_A1g00972	Ls_CBS5930|g5100.t1;Ls_CBS5931|g238.t1	0.0065	hypothetical protein
MvSI-1064-A1-R4_A1g00997	Ls_CBS5930|g1916.t1;Ls_CBS5931|g98.t1	0.0062	hypothetical protein
MvSI-1064-A1-R4_A1g00998	Ls_CBS5930|g3566.t1;Ls_CBS5931|g147.t1	0.1334	U3 small nucleolar ribonucleoprotein IMP3 / Ribosomal protein S4/S9
MvSI-1064-A1-R4_A1g01017	Ls_CBS5930|g3407.t1;Ls_CBS5931|g8158.t1	0.0516	phosphatidylethanolamine N-methyltransferase (PEMT)
MvSI-1064-A1-R4_A1g01154	Ls_CBS5930|g5411.t1|corr;Ls_CBS5931|g3145.t1	0.0786	ribosomal protein L1
MvSI-1064-A1-R4_A1g01159	Ls_CBS5930|g3515.t1;Ls_CBS5931|g197.t1	0.0000	bZIP transcription factor (AP-1)
MvSI-1064-A1-R4_A1g01160	Ls_CBS5930|g5395.t1;Ls_CBS5931|g3159.t1	0.0239	COP9 signalosome complex subunit 2
MvSI-1064-A1-R4_A1g01161	Ls_CBS5930|g6628.t1;Ls_CBS5931|g3769.t1	0.0000	mitochondrial carrier protein
MvSI-1064-A1-R4_A1g01162	Ls_CBS5930|g5385.t1;Ls_CBS5931|g3169.t1	0.0986	hypothetical protein
MvSI-1064-A1-R4_A1g01163	Ls_CBS5930|g6627.t1;Ls_CBS5931|g3770.t1	0.0000	ADP-ribosylation factor-like protein 2
MvSI-1064-A1-R4_A1g01388	Ls_CBS5930|g4892.t1|corr;Ls_CBS5931|g6975.t1|corr	0.0948	ribosome assembly protein Noc2
MvSI-1064-A1-R4_A1g01440	Ls_CBS5930|g3762.t1;Ls_CBS5931|g4607.t1	0.0000	autophagy-related protein 7 / E1-like protein-activating enzyme Gsa7p/Apg7p
MvSI-1064-A1-R4_A1g01441	Ls_CBS5930|g3507.t1;Ls_CBS5931|g205.t1	0.0000	zinc finger, C3HC4 RING-type protein
MvSI-1064-A1-R4_A1g01457	Ls_CBS5930|g6847.t1;Ls_CBS5931|g3790.t1	0.0022	unnamed protein product
MvSI-1064-A1-R4_A1g01458	Ls_CBS5930|g6847.t1;Ls_CBS5931|g3790.t1	0.0022	DNA-directed RNA polymerase III subunit RPC1

Table S3. Gene ID and putative function of the genes located in the different evolutionary strata in *Microbotryum lychnidis-dioicae* (MvSl) (shared with *M. lagerheimii* (MvSv) mating-type chromosomes). The two HD genes are highlighted in bold and grey. The d_S corresponds to synonymous divergence between alleles associated to the alternative mating types of the sequenced individual.

MvSl gene ID (a_1)	MvSv gene ID (a_1)	d_S in MvSl	d_S in MvSv	Stratum	Putative function
MvSl-1064-A1-R4_A1g01509	MvSv-1253-A1-R1_MC03g02122	0	0	PAR	"AutoIPR: IPR008926:Ribonucleotide reductase R1 subunit, N-terminal; IPR013346:Ribonucleotide reductase, class I , alpha subunit; IPR013350:Ribonucleotide reductase alpha chain;"
MvSl-1064-A1-R4_A1g01508	MvSv-1253-A1-R1_MC03g02123	0	0	PAR	AutoIPR: IPR010482:Peroxin/Dysferlin domain;
MvSl-1064-A1-R4_A1g01502	MvSv-1253-A1-R1_MC03g02124	0,002787	0	PAR	AutoIPR: IPR009053:Prefoldin;
MvSl-1064-A1-R4_A1g01501	MvSv-1253-A1-R1_MC03g02125	0	0	PAR	AutoIPR: IPR001805:Adenosine kinase;
MvSl-1064-A1-R4_A1g01500	MvSv-1253-A1-R1_MC03g02126	0	0	PAR	AutoIPR: IPR016024:Armadillo-type fold; IPR027159:Nuclear cap-binding protein subunit 1;
MvSl-1064-A1-R4_A1g01498	MvSv-1253-A1-R1_MC03g02130	0	0	PAR	AutoIPR: IPR005821:Ion transport domain;
MvSl-1064-A1-R4_A1g01497	MvSv-1253-A1-R1_MC03g02134	0	0	PAR	AutoIPR: IPR011992:EF-hand domain pair;
MvSl-1064-A1-R4_A1g01492	MvSv-1253-A1-R1_MC03g02142	0	0	PAR	
MvSl-1064-A1-R4_A1g01491	MvSv-1253-A1-R1_MC03g02144	0	0	PAR	
MvSl-1064-A1-R4_A1g01489	MvSv-1253-A1-R1_MC03g02148	0	0	PAR	"AutoIPR: IPR006110:RNA polymerase, subunit omega/K/RPABC2;"
MvSl-1064-A1-R4_A1g01488	MvSv-1253-A1-R1_MC03g02149	0	0	PAR	"AutoIPR: IPR022591:Transcription initiation factor TFIID subunit 1, domain of unknown function;"
MvSl-1064-A1-R4_A1g01487	MvSv-1253-A1-R1_MC03g02150	0	0	PAR	AutoIPR: IPR021709:Protein of unknown function DUF3292;
MvSl-1064-A1-R4_A1g01478	MvSv-1253-A1-R1_MC03g02153	0	0	PAR	
MvSl-1064-A1-R4_A1g01486	MvSv-1253-A1-R1_MC03g02154	0	0	PAR	AutoIPR: IPR022440:Conserved hypothetical protein CHP03788;
MvSl-1064-A1-R4_A1g01485	MvSv-1253-A1-R1_MC03g02155	0	0	PAR	AutoIPR: IPR001237:43kDa postsynaptic protein; IPR001623:DnaJ domain; IPR026901:DnaJ homologue subfamily C member 3;
MvSl-1064-A1-R4_A1g01474	MvSv-1253-A1-R1_MC03g02159	0	0	PAR	
MvSl-1064-A1-R4_A1g01476	MvSv-1253-A1-R1_MC03g02160	0	0	PAR	
MvSl-1064-A1-R4_A1g01477	MvSv-1253-A1-R1_MC03g02164	0	0	PAR	AutoIPR: IPR006994:Transcription factor 25;
MvSl-1064-A1-R4_A1g01484	MvSv-1253-A1-R1_MC03g02165	0	0	PAR	
MvSl-1064-A1-R4_A1g01473	MvSv-1253-A1-R1_MC03g02166	0	0	PAR	
MvSl-1064-A1-R4_A1g01472	MvSv-1253-A1-R1_MC03g02167	0	0	PAR	AutoIPR: IPR003162:Transcription initiation factor TAFII31; IPR009072:Histone-fold;
MvSl-1064-A1-R4_A1g01471	MvSv-1253-A1-R1_MC03g02168	0	0	PAR	AutoIPR: IPR007900:Transcription initiation factor TFIID component TAF4;
MvSl-1064-A1-R4_A1g01470	MvSv-1253-A1-R1_MC03g02170	0	0	PAR	
MvSl-1064-A1-R4_A1g01468	MvSv-1253-A1-R1_MC03g02172	0	0	PAR	
MvSl-1064-A1-R4_A1g01466	MvSv-1253-A1-R1_MC03g02174	0	0	PAR	
MvSl-1064-A1-R4_A1g01463	MvSv-1253-A1-R1_MC03g02180	0	0	PAR	
MvSl-1064-A1-R4_A1g01462	MvSv-1253-A1-R1_MC03g02181	0	0	PAR	"AutoIPR: IPR014624:Predicted 26S proteasome regulatory complex, non-ATPase subcomplex, subunit s5a, Plasmodium; IPR027040:Proteasome subunit Rpn10;"
MvSl-1064-A1-R4_A1g01461	MvSv-1253-A1-R1_MC03g02182	0	0	PAR	AutoIPR: IPR000456:Ribosomal protein L17;
MvSl-1064-A1-R4_A1g01460	MvSv-1253-A1-R1_MC03g02183	0	0	PAR	
MvSl-1064-A1-R4_A1g01458	MvSv-1253-A1-R1_MC03g02185	0	0,01838	PAR	"AutoIPR: IPR009010:Aspartate decarboxylase-like domain; IPR012754:DNA-directed RNA polymerase, subunit beta-prime; IPR015700:DNA-directed RNA polymerase III largest subunit;"
MvSl-1064-A1-R4_A1g01457	MvSv-1253-A1-R1_MC03g02186	0	0,02487	PAR	
MvSl-1064-A1-R4_A1g01456	MvSv-1253-A1-R1_MC03g02187	0	0	PAR	
MvSl-1064-A1-R4_A1g01455	MvSv-1253-A1-R1_MC03g02188	0	0	PAR	
MvSl-1064-A1-R4_A1g01454	MvSv-1253-A1-R1_MC03g02189	0	0	PAR	
MvSl-1064-A1-R4_A1g01453	MvSv-1253-A1-R1_MC03g02190	0	0	PAR	"AutoIPR: IPR005828:General substrate transporter; IPR016196:Major facilitator superfamily domain, general substrate transporter;"
MvSl-1064-A1-R4_A1g01451	MvSv-1253-A1-R1_MC03g02191	0	0	PAR	"AutoIPR: IPR011042:Six-bladed beta-propeller, TolB-like;"
MvSl-1064-A1-R4_A1g01450	MvSv-1253-A1-R1_MC03g02192	0	0	PAR	"AutoIPR: IPR009082:Signal transduction histidine kinase, homodimeric domain; IPR011006:CheY-like superfamily; IPR013655:PAS fold-3; IPR014285:Nitrogen fixation negative regulator NifL;"
MvSl-1064-A1-R4_A1g01447	MvSv-1253-A1-R1_MC03g02193	0	0	PAR	"AutoIPR: IPR017923:Transcription factor IIS, N-terminal;"
MvSl-1064-A1-R4_A1g01446	MvSv-1253-A1-R1_MC03g02194	0	0	PAR	
MvSl-1064-A1-R4_A1g01445	MvSv-1253-A1-R1_MC03g02195	0	0	PAR	
MvSl-1064-A1-R4_A1g01444	MvSv-1253-A1-R1_MC03g02196	0	0	PAR	"AutoIPR: IPR002226:Catalase haem-binding site; IPR010582:Catalase immune-responsive domain; IPR011614:Catalase core domain; IPR018028:Catalase, mono-functional, haem-containing; IPR020835:Catalase-like domain; IPR024708:Catalase active site;"

MvSl gene ID (a_1)	MvSv gene ID (a_1)	d_S in MvSl	d_S in MvSv	Stratum	Putative function
MvSl-1064-A1-R4_A1g01441	MvSv-1253-A1-R1_MC03g02203	0	0,00184	blue	"AutoIPR: IPR013083:Zinc finger, RING/FYVE/PHD-type;"
MvSl-1064-A1-R4_A1g01440	MvSv-1253-A1-R1_MC03g02204	0	0,008478	blue	"AutoIPR: IPR006285:Ubiquitin-like modifier-activating enzyme Atg7; IPR018075:Ubiquitin-activating enzyme, E1;"
MvSl-1064-A1-R4_A1g01163	MvSv-1253-A1-R1_MC03g02211	0,04476	0,009024	blue	"AutoIPR: IPR005225:Small GTP-binding protein domain; IPR006689:Small GTPase superfamily, ARF/SAR type; IPR027417:P-loop containing nucleoside triphosphate hydrolase;"
MvSl-1064-A1-R4_A1g01162	MvSv-1253-A1-R1_MC03g02212	0,02929	0,0101	blue	
MvSl-1064-A1-R4_A1g01161	MvSv-1253-A1-R1_MC03g02213	0,00892	0,01558	blue	AutoIPR: IPR023395:Mitochondrial carrier domain;
MvSl-1064-A1-R4_A1g01160	MvSv-1253-A1-R1_MC03g02214	0,002244	0,03034	blue	AutoIPR: IPR000717:Proteasome component (PCI) domain; IPR011990:Tetratricopeptide-like helical; IPR013143:PCI/PINT associated module;
MvSl-1064-A1-R4_A1g01159	MvSv-1253-A1-R1_MC03g02215	0,02168	0,0225	blue	AutoIPR: IPR004827:Basic-leucine zipper domain; IPR013910:Transcription factor PAP1; IPR023167:Yap1 redox domain;
MvSl-1064-A1-R4_A1g01154	MvSv-1253-A1-R1_MC03g02216	0,005776	0,0116	blue	
MvSl-1064-A1-R4_A1g00659	MvSv-1253-A1-R1_MC03g02219	0,04854	0,008824	blue	AutoIPR: IPR022751:Alpha-mannosyltransferase;
MvSl-1064-A1-R4_A1g00800	MvSv-1253-A1-R1_MC03g02223	0,03416	0,007407	blue	"AutoIPR: IPR002085:Alcohol dehydrogenase superfamily, zinc-type; IPR016040:NAD(P)-binding domain; IPR020843:Polyketide synthase, enoylreductase;"
MvSl-1064-A1-R4_A1g00801	MvSv-1253-A1-R1_MC03g02224	0	0,0222	blue	AutoIPR: IPR007146:Sas10/Utp3/C1D; IPR011082:Exosome-associated factor Rrp47/DNA strand repair C1D;
MvSl-1064-A1-R4_A1g00808	MvSv-1253-A1-R1_MC03g02226	0,6698	0,02125	blue	
MvSl-1064-A1-R4_A1g00591	**MvSv-1253-A1-R1_MC03g02227**	**0,3894**	**0,4844**	**blue**	**AutoIPR: IPR008422:Homeobox KN domain; IPR009057:Homeodomain-like; HD gene**
MvSl-1064-A1-R4_A1g00592	**MvSv-1253-A1-R1_MC03g02228**	**0,8506**	**0,669**	**blue**	**HD gene**
MvSl-1064-A1-R4_A1g00593	MvSv-1253-A1-R1_MC03g02229	0,04204	0,03775	blue	AutoIPR: IPR027073:5'-3' exoribonuclease;
MvSl-1064-A1-R4_A1g00772	MvSv-1253-A1-R1_MC03g02230	0,03975	0,005973	blue	"AutoIPR: IPR012677:Nucleotide-binding, alpha-beta plait;"
MvSl-1064-A1-R4_A1g00025	MvSv-1253-A1-R1_MC03g02235	0	0,01151	blue	"AutoIPR: IPR000743:Glycoside hydrolase, family 28; IPR011050:Pectin lyase fold/virulence factor;"
MvSl-1064-A1-R4_A1g00478	MvSv-1253-A1-R1_MC03g02236	0,09438	0,03602	blue	AutoIPR: IPR012336:Thioredoxin-like fold;
MvSl-1064-A1-R4_A1g00495	MvSv-1253-A1-R1_MC03g02237	0,06234	0,01041	blue	"AutoIPR: IPR012677:Nucleotide-binding, alpha-beta plait;"
MvSl-1064-A1-R4_A1g01431	MvSv-1253-A1-R1_MC03g02238	0,03381	0	blue	"AutoIPR: IPR001752:Kinesin, motor domain; IPR008984:SMAD/FHA domain; IPR011993:Pleckstrin homology-like domain; IPR022164:Kinesin-like; IPR027417:P-loop containing nucleoside triphosphate hydrolase; IPR027640:Kinesin-like protein;"
MvSl-1064-A1-R4_A1g00997	MvSv-1253-A1-R1_MC03g02240	0,03601	0,01086	blue	
MvSl-1064-A1-R4_A1g00998	MvSv-1253-A1-R1_MC03g02241	0,03152	0,004411	blue	AutoIPR: IPR022801:Ribosomal protein S4/S9;
MvSl-1064-A1-R4_A1g00972	MvSv-1253-A1-R1_MC03g02242	0,01747	0,0052	blue	
MvSl-1064-A1-R4_A1g00971	MvSv-1253-A1-R1_MC03g02243	0,02441	0,02234	blue	AutoIPR: IPR000326:Phosphatidic acid phosphatase type 2/haloperoxidase;
MvSl-1064-A1-R4_A1g00970	MvSv-1253-A1-R1_MC03g02244	0,01335	0,01239	blue	AutoIPR: IPR002423:Chaperonin Cpn60/TCP-1; IPR027409:GroEL-like apical domain; IPR027410:TCP-1-like chaperonin intermediate domain; IPR027413:GroEL-like equatorial domain;
MvSl-1064-A1-R4_A1g00960	MvSv-1253-A1-R1_MC03g02248	0,03457	0	black	AutoIPR: IPR005024:Snf7;
MvSl-1064-A1-R4_A1g00958	MvSv-1253-A1-R1_MC03g02249	0,0192	0	black	AutoIPR: IPR004000:Actin-related protein;
MvSl-1064-A1-R4_A1g00957	MvSv-1253-A1-R1_MC03g02250	0,0344	0	black	AutoIPR: IPR013926:CGI121/TPRKB;
MvSl-1064-A1-R4_A1g00956	MvSv-1253-A1-R1_MC03g02251	0,05355	0	black	
MvSl-1064-A1-R4_A1g00955	MvSv-1253-A1-R1_MC03g02252	0,1164	0	black	
MvSl-1064-A1-R4_A1g00922	MvSv-1253-A1-R1_MC03g02253	0,04901	0	black	
MvSl-1064-A1-R4_A1g00921	MvSv-1253-A1-R1_MC03g02254	0,02868	0,003722	black	AutoIPR: IPR008942:ENTH/VHS;
MvSl-1064-A1-R4_A1g00920	MvSv-1253-A1-R1_MC03g02255	0,03374	0	black	
MvSl-1064-A1-R4_A1g00913	MvSv-1253-A1-R1_MC03g02256	0,06733	0,000814	black	AutoIPR: IPR012943:Spindle associated; IPR024545:Mto2p-binding domain;
MvSl-1064-A1-R4_A1g00912	MvSv-1253-A1-R1_MC03g02260	0	0	black	AutoIPR: IPR003782:Copper chaperone SCO1/SenC; IPR012336:Thioredoxin-like fold;
MvSl-1064-A1-R4_A1g00911	MvSv-1253-A1-R1_MC03g02261	0,01205	0	black	"AutoIPR: IPR008698:NADH:ubiquinone oxidoreductase, B18 subunit;"
MvSl-1064-A1-R4_A1g00794	MvSv-1253-A1-R1_MC03g02262	0,02735	0	black	AutoIPR: IPR009846:Splicing factor 3B subunit 5/RDS3 complex subunit 10;
MvSl-1064-A1-R4_A1g00644	MvSv-1253-A1-R1_MC03g02267	0,03817	0	black	"AutoIPR: IPR000571:Zinc finger, CCCH-type;"
MvSl-1064-A1-R4_A1g00645	MvSv-1253-A1-R1_MC03g02268	0,0177	0	black	AutoIPR: IPR001138:Zn(2)-C6 fungal-type DNA-binding domain;
MvSl-1064-A1-R4_A1g00646	MvSv-1253-A1-R1_MC03g02269	0,01013	0	black	AutoIPR: IPR012908:GPI inositol-deacylase PGAP1-like;
MvSl-1064-A1-R4_A1g00647	MvSv-1253-A1-R1_MC03g02270	0,07508	0	black	"AutoIPR: IPR007541:Uncharacterised protein family, basic secretory protein;"
MvSl-1064-A1-R4_A1g00648	MvSv-1253-A1-R1_MC03g02271	0,02229	0	black	"AutoIPR: IPR019339:CBF1-interacting co-repressor CIR, N-terminal domain; IPR022209:Pre-mRNA splicing factor;"
MvSl-1064-A1-R4_A1g01129	MvSv-1253-A1-R1_MC03g02273	0,05174	0	black	AutoIPR: IPR008978:HSP20-like chaperone;
MvSl-1064-A1-R4_A1g00311	MvSv-1253-A1-R1_MC03g02276	0,02807	0	black	AutoIPR: IPR015915:Kelch-type beta propeller;
MvSl-1064-A1-R4_A1g00312	MvSv-1253-A1-R1_MC03g02277	0,02654	0	black	"AutoIPR: IPR019191:Essential protein Yae1, N-terminal;"
MvSl-1064-A1-R4_A1g00886	MvSv-1253-A1-R1_MC03g02280	0,03442	0	black	
MvSl-1064-A1-R4_A1g00869	MvSv-1253-A1-R1_MC03g02282	0,04332	0	black	"AutoIPR: IPR006003:Carbohydrate kinase, FGGY-related;"

MvSl gene ID (a_1)	MvSv gene ID (a_1)	d_S in MvSl	d_S in MvSv	Stratum	Putative function
MvSl-1064-A1-R4_A1g01135	MvSv-1253-A1-R1_MC16g09520	0,05381	0	black	"AutoIPR: IPR019400:Peptidase C65, otubain;"
MvSl-1064-A1-R4_A1g01136	MvSv-1253-A1-R1_MC16g09519	0,0594	0	black	
MvSl-1064-A1-R4_A1g01137	MvSv-1253-A1-R1_MC16g09518	0,02957	0	black	
MvSl-1064-A1-R4_A1g00732	MvSv-1253-A1-R1_MC16g09516	0,002396	0	black	
MvSl-1064-A1-R4_A1g01407	MvSv-1253-A1-R1_MC16g09514	0,02369	0	black	
MvSl-1064-A1-R4_A1g01406	MvSv-1253-A1-R1_MC16g09512	0,002257	0	black	AutoIPR: IPR007757:MT-A70-like;
MvSl-1064-A1-R4_A1g01405	MvSv-1253-A1-R1_MC16g09511	0,01406	0	black	AutoIPR: IPR027450:Alpha-ketoglutarate-dependent dioxygenase AlkB-like;
MvSl-1064-A1-R4_A1g01404	MvSv-1253-A1-R1_MC16g09510	0,05471	0	black	
MvSl-1064-A1-R4_A1g00326	MvSv-1253-A1-R1_MC16g09508	0,04389	0	black	
MvSl-1064-A1-R4_A1g00327	MvSv-1253-A1-R1_MC16g09507	0,02724	0	black	
MvSl-1064-A1-R4_A1g00448	MvSv-1253-A1-R1_MC16g09503	0,06255	0	black	
MvSl-1064-A1-R4_A1g00749	MvSv-1253-A1-R1_MC16g09501	0,02509	0	black	
MvSl-1064-A1-R4_A1g00750	MvSv-1253-A1-R1_MC16g09500	0,002806	0	black	
MvSl-1064-A1-R4_A1g00751	MvSv-1253-A1-R1_MC16g09499	0,01061	0	black	
MvSl-1064-A1-R4_A1g00752	MvSv-1253-A1-R1_MC16g09498	0,07687	0	black	
MvSl-1064-A1-R4_A1g00755	MvSv-1253-A1-R1_MC16g09497	0,07173	0	black	
MvSl-1064-A1-R4_A1g00757	MvSv-1253-A1-R1_MC16g09496	0,05103	0	black	AutoIPR: IPR001461:Peptidase A1; IPR021109:Aspartic peptidase;
MvSl-1064-A1-R4_A1g00544	MvSv-1253-A1-R1_MC16g09494	0,007251	0	black	"AutoIPR: IPR010032:FAD-linked oxidoreductase; IPR016166:FAD-binding, type 2; IPR023595:L-gulonolactone/D-arabinono-1,4-lactone oxidase;"
MvSl-1064-A1-R4_A1g00543	MvSv-1253-A1-R1_MC16g09493	0	0	black	AutoIPR: IPR016460:Coatomer beta subunit (COPB1); IPR026739:AP complex subunit beta;
MvSl-1064-A1-R4_A1g00542	MvSv-1253-A1-R1_MC16g09492	0,002593	0	black	AutoIPR: IPR001737:Ribosomal RNA adenine methylase transferase; IPR025814:18S rRNA dimethylase DIM1;
MvSl-1064-A1-R4_A1g00541	MvSv-1253-A1-R1_MC16g09488	0,01331	0	black	AutoIPR: IPR024990:Anaphase-promoting complex subunit 1;
MvSl-1064-A1-R4_A1g00534	MvSv-1253-A1-R1_MC16g09487	0	0	black	AutoIPR: IPR001557:L-lactate/malate dehydrogenase;
MvSl-1064-A1-R4_A1g00533	MvSv-1253-A1-R1_MC16g09486	0,07944	0	black	"AutoIPR: IPR011234:Fumarylacetoacetase, C-terminal-related;"
MvSl-1064-A1-R4_A1g00532	MvSv-1253-A1-R1_MC16g09485	0,0261	0	black	
MvSl-1064-A1-R4_A1g00528	MvSv-1253-A1-R1_MC16g09482	0,02956	0	black	
MvSl-1064-A1-R4_A1g00525	MvSv-1253-A1-R1_MC16g09479	0,02199	0,01648	black	
MvSl-1064-A1-R4_A1g00522	MvSv-1253-A1-R1_MC16g09478	0,04318	0,01311	black	"AutoIPR: IPR011701:Major facilitator superfamily; IPR016196:Major facilitator superfamily domain, general substrate transporter;"
MvSl-1064-A1-R4_A1g00521	MvSv-1253-A1-R1_MC16g09477	0,002238	0,002248	black	AutoIPR: IPR013126:Heat shock protein 70 family;
MvSl-1064-A1-R4_A1g00520	MvSv-1253-A1-R1_MC16g09476	0	0,02046	black	
MvSl-1064-A1-R4_A1g00519	MvSv-1253-A1-R1_MC16g09475	0	0,01423	black	"AutoIPR: IPR011016:Zinc finger, RING-CH-type; IPR013083:Zinc finger, RING/FYVE/PHD-type;"
MvSl-1064-A1-R4_A1g00518	MvSv-1253-A1-R1_MC16g09474	0,002431	0,01173	black	AutoIPR: IPR011047:Quinonprotein alcohol dehydrogenase-like superfamily; IPR015943:WD40/YVTN repeat-like-containing domain;
MvSl-1064-A1-R4_A1g00517	MvSv-1253-A1-R1_MC16g09473	0	0	black	
MvSl-1064-A1-R4_A1g00516	MvSv-1253-A1-R1_MC16g09472	0,02563	0,01878	black	"AutoIPR: IPR007087:Zinc finger, C2H2; IPR015940:Ubiquitin-associated/translation elongation factor EF1B, N-terminal, eukaryote; IPR017346:Uncharacterised conserved protein UCP037991, UAS/UBX;"
MvSl-1064-A1-R4_A1g00515	MvSv-1253-A1-R1_MC16g09471	0,01326	0,02447	black	"AutoIPR: IPR006293:DNA helicase, ATP-dependent, RecQ type, bacterial; IPR027417:P-loop containing nucleoside triphosphate hydrolase;"
MvSl-1064-A1-R4_A1g00514	MvSv-1253-A1-R1_MC16g09470	0,02296	0,02073	black	AutoIPR: IPR008936:Rho GTPase activation protein;
MvSl-1064-A1-R4_A1g00513	MvSv-1253-A1-R1_MC16g09469	0,0009531	0,01438	black	AutoIPR: IPR008521:Magnesium transporter NIPA;
MvSl-1064-A1-R4_A1g00512	MvSv-1253-A1-R1_MC16g09468	0	0,02597	black	"AutoIPR: IPR007305:Vesicle transport protein, Got1/SFT2-like;"
MvSl-1064-A1-R4_A1g00511	MvSv-1253-A1-R1_MC16g09467	0	0,03902	black	AutoIPR: IPR023395:Mitochondrial carrier domain;
MvSl-1064-A1-R4_A1g00510	MvSv-1253-A1-R1_MC16g09466	0	0,01317	black	"AutoIPR: IPR003754:Tetrapyrrole biosynthesis, uroporphyrinogen III synthase;"
MvSl-1064-A1-R4_A1g00509	MvSv-1253-A1-R1_MC16g09465	0,09326	0,02499	black	AutoIPR: IPR003817:Phosphatidylserine decarboxylase-related;
MvSl-1064-A1-R4_A1g00508	MvSv-1253-A1-R1_MC16g09464	0,1019	0,01383	black	"AutoIPR: IPR002938:Monooxygenase, FAD-binding; IPR020946:Flavin monooxygenase-like;"
MvSl-1064-A1-R4_A1g00506	MvSv-1253-A1-R1_MC16g09461	0,004505	0	black	AutoIPR: IPR002791:Domain of unknown function DUF89;
MvSl-1064-A1-R4_A1g00505	MvSv-1253-A1-R1_MC16g09460	0	0,01273	black	"AutoIPR: IPR005097:Saccharopine dehydrogenase / Homospermidine synthase; IPR007698:Alanine dehydrogenase/PNT, NAD(H)-binding domain; IPR007886:Alanine dehydrogenase/pyridine nucleotide transhydrogenase, N-terminal;"
MvSl-1064-A1-R4_A1g00503	MvSv-1253-A1-R1_MC16g09459	0,009071	0,01064	black	AutoIPR: IPR008942:ENTH/VHS; IPR018205:VHS subgroup;
MvSl-1064-A1-R4_A1g01351	MvSv-1253-A1-R1_MC16g09458	0,003649	0	black	AutoIPR: IPR001189:Manganese/iron superoxide dismutase;
MvSl-1064-A1-R4_A1g01350	MvSv-1253-A1-R1_MC16g09457	0,01323	0	black	AutoIPR: IPR024338:Stretch-activated cation channel Mid1;
MvSl-1064-A1-R4_A1g01348	MvSv-1253-A1-R1_MC16g09456	0,0105	0	black	AutoIPR: IPR000387:Protein-tyrosine/Dual specificity phosphatase; IPR008343:Mitogen-activated protein (MAP) kinase phosphatase; IPR024950:Dual specificity phosphatase;

MvSl gene ID (a_1)	MvSv gene ID (a_1)	d_S in MvSl	d_S in MvSv	Stratum	Putative function
MvSl-1064-A1-R4_A1g01347	MvSv-1253-A1-R1_MC16g09455	0,02952	0	black	"AutoIPR: IPR012954:BP28, C-terminal domain; IPR016024:Armadillo-type fold; IPR022125:U3 small nucleolar RNA-associated protein 10;"
MvSl-1064-A1-R4_A1g01415	MvSv-1253-A1-R1_MC16g09444	0,02235	0	black	"AutoIPR: IPR008352:Mitogen-activated protein (MAP) kinase, p38; IPR020777:Tyrosine-protein kinase, neurotrophic receptor;"
MvSl-1064-A1-R4_A1g01393	MvSv-1253-A1-R1_MC16g09443	0,03313	0	black	
MvSl-1064-A1-R4_A1g01392	MvSv-1253-A1-R1_MC16g09442	0,02447	0	black	
MvSl-1064-A1-R4_A1g01479	MvSv-1253-A1-R1_MC16g09439	0	0	black	
MvSl-1064-A1-R4_A1g00211	MvSv-1253-A1-R1_MC12g07980	0,01398	0	black	"AutoIPR: IPR008010:Membrane protein,Tapt1/CMV receptor;"
MvSl-1064-A1-R4_A1g00779	MvSv-1253-A1-R1_MC12g07965	0,04375	0	black	AutoIPR: IPR005378:Vacuolar protein sorting-associated protein 35;
MvSl-1064-A1-R4_A1g00778	MvSv-1253-A1-R1_MC12g07964	0,04144	0	black	"AutoIPR: IPR015408:Zinc finger, Mcm10/DnaG-type;"
MvSl-1064-A1-R4_A1g00241	MvSv-1253-A1-R1_MC12g07960	0,03193	0	black	
MvSl-1064-A1-R4_A1g00242	MvSv-1253-A1-R1_MC12g07959	0,033	0	black	AutoIPR: IPR007653:Signal peptidase 22kDa subunit;
MvSl-1064-A1-R4_A1g00245	MvSv-1253-A1-R1_MC12g07956	0,07408	0	black	
MvSl-1064-A1-R4_A1g00269	MvSv-1253-A1-R1_MC12g07952	0,04395	0	black	"AutoIPR: IPR003111:Peptidase S16, lon N-terminal; IPR014252:Sporulation protease LonC; IPR014721:Ribosomal protein S5 domain 2-type fold, subgroup; IPR015947:PUA-like domain; IPR027065:Lon protease; IPR027417:P-loop containing nucleoside triphosphate hydrolase;"
MvSl-1064-A1-R4_A1g00270	MvSv-1253-A1-R1_MC12g07950	0,04929	0	black	"AutoIPR: IPR006219:DHAP synthase, class 1; IPR013785:Aldolase-type TIM barrel;"
MvSl-1064-A1-R4_A1g00292	MvSv-1253-A1-R1_MC12g07947	0,02908	0	black	AutoIPR: IPR001394:Ubiquitin carboxyl-terminal hydrolases family 2; IPR019955:Ubiquitin supergroup;
MvSl-1064-A1-R4_A1g00290	MvSv-1253-A1-R1_MC12g07946	0,02661	0	black	AutoIPR: IPR027815:Domain of unknown function DUF4463;
MvSl-1064-A1-R4_A1g00693	MvSv-1253-A1-R1_MC12g07943	0	0	black	AutoIPR: IPR002042:Uricase;
MvSl-1064-A1-R4_A1g00694	MvSv-1253-A1-R1_MC12g07942	0,01544	0	black	"AutoIPR: IPR002100:Transcription factor, MADS-box;"
MvSl-1064-A1-R4_A1g00719	MvSv-1253-A1-R1_MC12g07935	0,1062	0	black	"AutoIPR: IPR004589:DNA helicase, ATP-dependent, RecQ type; IPR018973:DEAD/DEAH-box helicase, putative; IPR027417:P-loop containing nucleoside triphosphate hydrolase;"
MvSl-1064-A1-R4_A1g00718	MvSv-1253-A1-R1_MC12g07934	0,03731	0	black	"AutoIPR: IPR007577:Glycosyltransferase, DXD sugar-binding motif;"
MvSl-1064-A1-R4_A1g00254	MvSv-1253-A1-R1_MC12g07933	0,03514	0	black	AutoIPR: IPR003386:Lecithin:cholesterol/phospholipid:diacylglycerol acyltransferase;
MvSl-1064-A1-R4_A1g00359	MvSv-1253-A1-R1_MC12g07932	0,02437	0	black	AutoIPR: IPR020831:Glyceraldehyde/Erythrose phosphate dehydrogenase family;
MvSl-1064-A1-R4_A1g00281	MvSv-1253-A1-R1_MC12g07931	0,04624	0	black	"AutoIPR: IPR003959:ATPase, AAA-type, core; IPR027417:P-loop containing nucleoside triphosphate hydrolase;"
MvSl-1064-A1-R4_A1g00280	MvSv-1253-A1-R1_MC12g07930	0,02891	0	black	"AutoIPR: IPR008973:C2 calcium/lipid-binding domain, CaLB; IPR019558:Mammalian uncoordinated homology 13, subgroup, domain 2;"
MvSl-1064-A1-R4_A1g00433	MvSv-1253-A1-R1_MC12g07928	0,02267	0,001815	black	"AutoIPR: IPR022042:snRNA-activating protein complex, subunit 3;"
MvSl-1064-A1-R4_A1g00432	MvSv-1253-A1-R1_MC12g07927	0,1063	0	black	AutoIPR: IPR009071:High mobility group box domain;
MvSl-1064-A1-R4_A1g00349	MvSv-1253-A1-R1_MC12g07926	0,09006	0	black	AutoIPR: IPR000791:GPR1/FUN34/yaaH;
MvSl-1064-A1-R4_A1g00350	MvSv-1253-A1-R1_MC12g07925	0,02792	0	black	AutoIPR: IPR015915:Kelch-type beta propeller;
MvSl-1064-A1-R4_A1g00351	MvSv-1253-A1-R1_MC12g07924	0,03002	0,0007955	black	"AutoIPR: IPR007320:Programmed cell death protein 2, C-terminal; IPR015940:Ubiquitin-associated/translation elongation factor EF1B, N-terminal, eukaryote; IPR017346:Uncharacterised conserved protein UCP037991, UAS/UBX;"
MvSl-1064-A1-R4_A1g00352	MvSv-1253-A1-R1_MC12g07923	0,03106	0,006247	black	"AutoIPR: IPR016656:Transcription initiation factor TFIIE, beta subunit;"
MvSl-1064-A1-R4_A1g01272	MvSv-1253-A1-R1_MC12g07922	0,01626	0	black	AutoIPR: IPR008417:B-cell receptor-associated 31-like;
MvSl-1064-A1-R4_A1g01271	MvSv-1253-A1-R1_MC12g07921	0,01543	0	black	AutoIPR: IPR008011:Complex 1 LYR protein;
MvSl-1064-A1-R4_A1g01173	MvSv-1253-A1-R1_MC12g07920	0,03657	0,007907	black	"AutoIPR: IPR012677:Nucleotide-binding, alpha-beta plait;"
MvSl-1064-A1-R4_A1g01174	MvSv-1253-A1-R1_MC12g07919	0,02616	0	black	AutoIPR: IPR014729:Rossmann-like alpha/beta/alpha sandwich fold;
MvSl-1064-A1-R4_A1g01220	MvSv-1253-A1-R1_MC12g07918	0,09423	0	black	"AutoIPR: IPR001781:Zinc finger, LIM-type;"
MvSl-1064-A1-R4_A1g01219	MvSv-1253-A1-R1_MC12g07917	0,06024	0	black	AutoIPR: IPR018803:Stress-responsive protein Ish1;
MvSl-1064-A1-R4_A1g00165	MvSv-1253-A1-R1_MC12g07913	0,03698	0,00352	black	"AutoIPR: IPR006153:Cation/H+ exchanger; IPR018422:Cation/H+ exchanger, CPA1 family;"
MvSl-1064-A1-R4_A1g00157	MvSv-1253-A1-R1_MC12g07911	0,03635	0,01021	black	"AutoIPR: IPR016196:Major facilitator superfamily domain, general substrate transporter;"
MvSl-1064-A1-R4_A1g00155	MvSv-1253-A1-R1_MC12g07910	0,04423	0	black	AutoIPR: IPR001645:Folylpolyglutamate synthetase;
MvSl-1064-A1-R4_A1g00153	MvSv-1253-A1-R1_MC12g07908	0,03147	0,003478	black	"AutoIPR: IPR010222:RNA helicase, ATP-dependent DEAH box, HrpA-type; IPR022307:DEAD/DEAH-box helicase, putative, actinobacteria; IPR027417:P-loop containing nucleoside triphosphate hydrolase;"
MvSl-1064-A1-R4_A1g01212	MvSv-1253-A1-R1_MC12g07907	0,03602	0,002255	black	"AutoIPR: IPR001208:Mini-chromosome maintenance, DNA-dependent ATPase; IPR027417:P-loop containing nucleoside triphosphate hydrolase; IPR027925:MCM N-terminal domain;"
MvSl-1064-A1-R4_A1g01184	MvSv-1253-A1-R1_MC12g07904	0,03576	0,006311	black	AutoIPR: IPR001708:Membrane insertase OXA1/ALB3/YidC;
MvSl-1064-A1-R4_A1g01189	MvSv-1253-A1-R1_MC12g07903	0,02386	0	black	"AutoIPR: IPR011598:Myc-type, basic helix-loop-helix (bHLH) domain;"
MvSl-1064-A1-R4_A1g00016	MvSv-1253-A1-R1_MC12g07897	0	0	black	
MvSl-1064-A1-R4_A1g00017	MvSv-1253-A1-R1_MC12g07896	0	0,01191	black	"AutoIPR: IPR011701:Major facilitator superfamily; IPR016196:Major facilitator superfamily domain, general substrate transporter;"
MvSl-1064-A1-R4_A1g00144	MvSv-1253-A1-R1_MC12g07894	0,05262	0	black	"AutoIPR: IPR006789:ARP2/3 complex, 16kDa subunit (p16-Arc);"

MvSl gene ID (a_1)	MvSv gene ID (a_1)	d_S in MvSl	d_S in MvSv	Stratum	Putative function
MvSl-1064-A1-R4_A1g01389	MvSv-1253-A1-R1_MC12g07893	0,03083	0	black	
MvSl-1064-A1-R4_A1g01388	MvSv-1253-A1-R1_MC12g07892	0,04141	0,00527	black	AutoIPR: IPR005343:Nucleolar complex protein 2;
MvSl-1064-A1-R4_A1g01385	MvSv-1253-A1-R1_MC12g07891	0,02823	0,001958	black	"AutoIPR: IPR009668:RNA polymerase I associated factor, A49-like;"
MvSl-1064-A1-R4_A1g01384	MvSv-1253-A1-R1_MC12g07890	0,0293	0,00419	black	AutoIPR: IPR001060:FCH domain; IPR018808:Muniscin C-terminal mu homology domain;
MvSl-1064-A1-R4_A1g01369	MvSv-1253-A1-R1_MC12g07886	0,02333	0,001781	black	AutoIPR: IPR005792:Protein disulphide isomerase; IPR012336:Thioredoxin-like fold;
MvSl-1064-A1-R4_A1g01368	MvSv-1253-A1-R1_MC12g07885	0,02638	0,005801	black	AutoIPR: IPR019021:Methyl methanesulphonate-sensitivity protein 22;
MvSl-1064-A1-R4_A1g01367	MvSv-1253-A1-R1_MC12g07884	0,01551	0,00982	black	
MvSl-1064-A1-R4_A1g01366	MvSv-1253-A1-R1_MC12g07883	0,0362	0,00599	black	AutoIPR: IPR006565:Bromodomain transcription factor;
MvSl-1064-A1-R4_A1g00845	MvSv-1253-A1-R1_MC12g07881	0,03648	0,001712	black	"AutoIPR: IPR008937:Ras guanine nucleotide exchange factor; IPR023578:Ras guanine nucleotide exchange factor, domain;"
MvSl-1064-A1-R4_A1g00844	MvSv-1253-A1-R1_MC12g07880	0,008035	0	black	
MvSl-1064-A1-R4_A1g00843	MvSv-1253-A1-R1_MC12g07879	0,0116	0,002791	black	AutoIPR: IPR002060:Squalene/phytoene synthase;
MvSl-1064-A1-R4_A1g00842	MvSv-1253-A1-R1_MC12g07878	0,06322	0	black	"AutoIPR: IPR002018:Carboxylesterase, type B;"
MvSl-1064-A1-R4_A1g00840	MvSv-1253-A1-R1_MC12g07874	0,04014	0,004762	black	
MvSl-1064-A1-R4_A1g00832	MvSv-1253-A1-R1_MC12g07872	0,02415	0,001244	black	AutoIPR: IPR011009:Protein kinase-like domain;
MvSl-1064-A1-R4_A1g00575	MvSv-1253-A1-R1_MC12g07870	0,02905	0,003192	black	AutoIPR: IPR002058:PAP/25A-associated; IPR002934:Nucleotidyl transferase domain;
MvSl-1064-A1-R4_A1g00569	MvSv-1253-A1-R1_MC12g07869	0,1057	0,04197	black	
MvSl-1064-A1-R4_A1g00093	MvSv-1253-A1-R1_MC12g07864	0,04154	0,006273	black	
MvSl-1064-A1-R4_A1g00186	MvSv-1253-A1-R1_MC12g07863	0,03298	0,01127	black	AutoIPR: IPR005013:Dolichyl-diphosphooligosaccharide--protein glycosyltransferase subunit WBP1;
MvSl-1064-A1-R4_A1g00185	MvSv-1253-A1-R1_MC12g07862	0,02174	0,002111	black	AutoIPR: IPR011047:Quinonprotein alcohol dehydrogenase-like superfamily; IPR026895:ER membrane protein complex subunit 1;
MvSl-1064-A1-R4_A1g00184	MvSv-1253-A1-R1_MC12g07861	0	0	black	"AutoIPR: IPR002222:Ribosomal protein S19/S15; IPR023575:Ribosomal protein S19, superfamily;"
MvSl-1064-A1-R4_A1g01038	MvSv-1253-A1-R1_MC12g07859	0,01992	0	black	AutoIPR: IPR000836:Phosphoribosyltransferase domain; IPR023031:Orotate phosphoribosyltransferase;
MvSl-1064-A1-R4_A1g01021	MvSv-1253-A1-R1_MC12g07856	0,02939	NA	black	
MvSl-1064-A1-R4_A1g00175	MvSv-1253-A1-R1_MC12g07851	0,1428	0,06338	purple	AutoIPR: IPR004147:UbiB domain;
MvSl-1064-A1-R4_A1g00279	MvSv-1253-A1-R1_MC12g07848	0,09067	NA	purple	
MvSl-1064-A1-R4_A1g00854	MvSv-1253-A1-R1_MC12g07846	0,02438	0,04877	purple	AutoIPR: IPR016024:Armadillo-type fold; IPR027140:Importin subunit beta;
MvSl-1064-A1-R4_A1g01227	MvSv-1253-A1-R1_MC12g07836	0,03955	0	purple	AutoIPR: IPR021138:Ribosomal protein L18a; IPR023573:Ribosomal protein L18a/LX;
MvSl-1064-A1-R4_A1g00230	MvSv-1253-A1-R1_MC12g07828	0,109	0,1148	purple	"AutoIPR: IPR006818:Histone chaperone, ASF1-like;"
MvSl-1064-A1-R4_A1g01017	MvSv-1253-A1-R1_MC12g07823	0,02769	0,07915	purple	AutoIPR: IPR007318:Phospholipid methyltransferase;
MvSl-1064-A1-R4_A1g00726	MvSv-1253-A1-R1_MC12g07815	0,1145	0,07136	purple	AutoIPR: IPR009060:UBA-like; IPR014764:Defective-in-cullin neddylation protein;
MvSl-1064-A1-R4_A1g00624	MvSv-1253-A1-R1_MC12g07792	0,08473	0,03743	purple	"AutoIPR: IPR016071:Staphylococcal nuclease (SNase-like), OB-fold;"
MvSl-1064-A1-R4_A1g00126	MvSv-1253-A1-R1_MC12g07780	0,4265	0,1397	purple	AutoIPR: IPR019166:Apolipoprotein O;
MvSl-1064-A1-R4_A1g00306	MvSv-1253-A1-R1_MC12g07758	NA	NA	orange	
MvSl-1064-A1-R4_A1g00307	MvSv-1253-A1-R1_MC12g07757	0,1172	0,004983	orange	AutoIPR: IPR000702:Ribosomal protein L6;
MvSl-1064-A1-R4_A1g00441	MvSv-1253-A1-R1_MC12g07755	0,03188	0,004631	orange	"AutoIPR: IPR009025:DNA-directed RNA polymerase, RBP11-like dimerisation domain; IPR011262:DNA-directed RNA polymerase, insert domain;"
MvSl-1064-A1-R4_A1g01253	MvSv-1253-A1-R1_MC12g07753	0,02466	0	orange	"AutoIPR: IPR009053:Prefoldin; IPR016655:Prefoldin, subunit 3;"
MvSl-1064-A1-R4_A1g01252	MvSv-1253-A1-R1_MC12g07752	0,07508	0,006777	orange	
MvSl-1064-A1-R4_A1g00669	MvSv-1253-A1-R1_MC12g07750	0,03217	0,002827	orange	"AutoIPR: IPR001876:Zinc finger, RanBP2-type; IPR007286:EAP30; IPR011991:Winged helix-turn-helix DNA-binding domain; IPR021648:Vacuolar protein sorting protein 36, GLUE domain;"
MvSl-1064-A1-R4_A1g01261	MvSv-1253-A1-R1_MC12g07749	0,03357	0,0004392	orange	"AutoIPR: IPR007309:B-block binding subunit of TFIIIC; IPR017956:AT hook, DNA-binding motif;"
MvSl-1064-A1-R4_A1g00407	MvSv-1253-A1-R1_MC12g07746	0,09576	0	red	AutoIPR: IPR000999:Ribonuclease III domain;
MvSl-1064-A1-R4_A1g00406	MvSv-1253-A1-R1_MC12g07745	0	0,01146	red	AutoIPR: IPR000307:Ribosomal protein S16; IPR023803:Ribosomal protein S16 domain;
MvSl-1064-A1-R4_A1g00405	MvSv-1253-A1-R1_MC12g07744	0,003614	0	red	AutoIPR: IPR015943:WD40/YVTN repeat-like-containing domain;
MvSl-1064-A1-R4_A1g00404	MvSv-1253-A1-R1_MC12g07742	0	0	red	AutoIPR: IPR013216:Methyltransferase type 11;
MvSl-1064-A1-R4_A1g00402	MvSv-1253-A1-R1_MC12g07740	0,01347	0,0006517	red	AutoIPR: IPR025279:Stress response protein NST1;
MvSl-1064-A1-R4_A1g00401	MvSv-1253-A1-R1_MC12g07739	0	0	red	AutoIPR: IPR002942:RNA-binding S4 domain; IPR022801:Ribosomal protein S4/S9;
MvSl-1064-A1-R4_A1g00399	MvSv-1253-A1-R1_MC12g07737	0	0	red	AutoIPR: IPR001147:Ribosomal protein L21e;
MvSl-1064-A1-R4_A1g00398	MvSv-1253-A1-R1_MC12g07736	0	0	red	"AutoIPR: IPR019711:ATPase, F0 complex, subunit H;"
MvSl-1064-A1-R4_A1g00397	MvSv-1253-A1-R1_MC12g07735	0	0	red	"AutoIPR: IPR007648:ATPase inhibitor, IATP, mitochondria;"
MvSl-1064-A1-R4_A1g00396	MvSv-1253-A1-R1_MC12g07734	0	0	red	"AutoIPR: IPR007482:Protein-tyrosine phosphatase-like, PTPLA;"
MvSl-1064-A1-R4_A1g00394	MvSv-1253-A1-R1_MC12g07732	0	0		

MvSl gene ID (a_1)	MvSv gene ID (a_1)	d_S in MvSl	d_S in MvSv	Stratum	Putative function
MvSl-1064-A1-R4_A1g00392	MvSv-1253-A1-R1_MC12g07731	0,03094	0	red	
MvSl-1064-A1-R4_A1g00391	MvSv-1253-A1-R1_MC12g07730	0,006953	0	red	"AutoIPR: IPR001392:Clathrin adaptor, mu subunit; IPR027059:Coatomer delta subunit;"
MvSl-1064-A1-R4_A1g00390	MvSv-1253-A1-R1_MC12g07729	0,008075	0	red	
MvSl-1064-A1-R4_A1g00384	MvSv-1253-A1-R1_MC12g07725	0,2181	0		
MvSl-1064-A1-R4_A1g00374	MvSv-1253-A1-R1_MC12g07723	0,001469	0,008644	red	AutoIPR: IPR009075:Acyl-CoA dehydrogenase/oxidase C-terminal; IPR012258:Acyl-CoA oxidase;
MvSl-1064-A1-R4_A1g00373	MvSv-1253-A1-R1_MC12g07722	0	0,02706	red	"AutoIPR: IPR020869:Exosome complex exonuclease 2, probable; IPR027408:PNPase/RNase PH domain;"
MvSl-1064-A1-R4_A1g00372	MvSv-1253-A1-R1_MC12g07721	0,002337	0,002394	red	"AutoIPR: IPR000924:Glutamyl/glutaminyl-tRNA synthetase, class Ib; IPR010987:Glutathione S-transferase, C-terminal-like;"
MvSl-1064-A1-R4_A1g00370	MvSv-1253-A1-R1_MC12g07719	0	0,01147	red	"AutoIPR: IPR007246:Gaa1-like, GPI transamidase component;"
MvSl-1064-A1-R4_A1g00369	MvSv-1253-A1-R1_MC12g07718	0,003175	0,001599	red	AutoIPR: IPR016161:Aldehyde/histidinol dehydrogenase;
MvSl-1064-A1-R4_A1g00368	MvSv-1253-A1-R1_MC12g07717	0,007024	0,002525	red	AutoIPR: IPR003358:tRNA (guanine-N-7) methyltransferase;
MvSl-1064-A1-R4_A1g00367	MvSv-1253-A1-R1_MC12g07716	0,003783	0	red	"AutoIPR: IPR011701:Major facilitator superfamily; IPR016196:Major facilitator superfamily domain, general substrate transporter;"
MvSl-1064-A1-R4_A1g00113	MvSv-1253-A1-R1_MC12g07715	0,007056	0	green	"AutoIPR: IPR002290:Serine/threonine- / dual specificity protein kinase, catalytic domain; IPR020777:Tyrosine-protein kinase, neurotrophic receptor;"
MvSl-1064-A1-R4_A1g00110	MvSv-1253-A1-R1_MC12g07712	0,001184	0	green	
MvSl-1064-A1-R4_A1g00109	MvSv-1253-A1-R1_MC12g07711	0,004364	0,04003	green	"AutoIPR: IPR012677:Nucleotide-binding, alpha-beta plait;"
MvSl-1064-A1-R4_A1g00080	MvSv-1253-A1-R1_MC12g07706	0	0	PAR	
MvSl-1064-A1-R4_A1g00078	MvSv-1253-A1-R1_MC12g07704	0	0	PAR	AutoIPR: IPR002672:Ribosomal protein L28e;
MvSl-1064-A1-R4_A1g00077	MvSv-1253-A1-R1_MC12g07703	0,009973	0,03064	PAR	AutoIPR: IPR004087:K Homology domain;
MvSl-1064-A1-R4_A1g00076	MvSv-1253-A1-R1_MC12g07702	0	0,002377	PAR	
MvSl-1064-A1-R4_A1g00075	MvSv-1253-A1-R1_MC12g07701	0	0,004902	PAR	"AutoIPR: IPR008928:Six-hairpin glycosidase-like; IPR010905:Glycosyl hydrolase, family 88;"
MvSl-1064-A1-R4_A1g00074	MvSv-1253-A1-R1_MC12g07700	0	0,0205	PAR	AutoIPR: IPR002791:Domain of unknown function DUF89;
MvSl-1064-A1-R4_A1g00073	MvSv-1253-A1-R1_MC12g07699	0	0,01967	PAR	AutoIPR: IPR013763:Cyclin-like;
MvSl-1064-A1-R4_A1g00072	MvSv-1253-A1-R1_MC12g07698	0	0,01032	PAR	AutoIPR: IPR002123:Phospholipid/glycerol acyltransferase;
MvSl-1064-A1-R4_A1g00071	MvSv-1253-A1-R1_MC12g07697	0	0	PAR	"AutoIPR: IPR012951:Berberine/berberine-like; IPR016166:FAD-binding, type 2;"
MvSl-1064-A1-R4_A1g00070	MvSv-1253-A1-R1_MC12g07696	0	0	PAR	AutoIPR: IPR009449:GDPGTP exchange factor Sec2p;
MvSl-1064-A1-R4_A1g00069	MvSv-1253-A1-R1_MC12g07695	0	0,0039	PAR	"AutoIPR: IPR020461:Tyrosine-protein kinase, neurotrophic receptor, type 1;"
MvSl-1064-A1-R4_A1g00068	MvSv-1253-A1-R1_MC12g07694	0	0	PAR	
MvSl-1064-A1-R4_A1g00067	MvSv-1253-A1-R1_MC12g07693	0	0,0214	PAR	
MvSl-1064-A1-R4_A1g00065	MvSv-1253-A1-R1_MC12g07691	0	0	PAR	AutoIPR: IPR012696:Phosphonate metabolism PhnM;
MvSl-1064-A1-R4_A1g00064	MvSv-1253-A1-R1_MC12g07683	0	0	PAR	
MvSl-1064-A1-R4_A1g00063	MvSv-1253-A1-R1_MC12g07682	0	0	PAR	"AutoIPR: IPR009244:Mediator complex, subunit Med7;"
MvSl-1064-A1-R4_A1g00062	MvSv-1253-A1-R1_MC12g07681	0	0	PAR	"AutoIPR: IPR012677:Nucleotide-binding, alpha-beta plait;"
MvSl-1064-A1-R4_A1g00061	MvSv-1253-A1-R1_MC12g07680	0	0	PAR	AutoIPR: IPR001806:Small GTPase superfamily; IPR002041:Ran GTPase; IPR005225:Small GTP-binding protein domain; IPR027417:P-loop containing nucleoside triphosphate hydrolase;
MvSl-1064-A1-R4_A1g00057	MvSv-1253-A1-R1_MC12g07678	0	0	PAR	
MvSl-1064-A1-R4_A1g00056	MvSv-1253-A1-R1_MC12g07677	0	0	PAR	"AutoIPR: IPR005828:General substrate transporter; IPR016196:Major facilitator superfamily domain, general substrate transporter;"
MvSl-1064-A1-R4_A1g00055	MvSv-1253-A1-R1_MC12g07676	0	0	PAR	AutoIPR: IPR013960:DASH complex subunit Duo1;role in spindle attachment, chromosome segregation and spindle stability.
MvSl-1064-A1-R4_A1g00054	MvSv-1253-A1-R1_MC12g07675	0	0	PAR	AutoIPR: IPR001269:tRNA-dihydrouridine synthase; IPR013785:Aldolase-type TIM barrel;
MvSl-1064-A1-R4_A1g00053	MvSv-1253-A1-R1_MC12g07674	0	0	PAR	AutoIPR: IPR012336:Thioredoxin-like fold;
MvSl-1064-A1-R4_A1g00052	MvSv-1253-A1-R1_MC12g07673	0	0	PAR	
MvSl-1064-A1-R4_A1g00051	MvSv-1253-A1-R1_MC12g07672	0	0	PAR	AutoIPR: IPR000760:Inositol monophosphatase;
MvSl-1064-A1-R4_A1g00050	MvSv-1253-A1-R1_MC12g07671	0	0	PAR	"AutoIPR: IPR002092:DNA-directed RNA polymerase, phage-type; IPR024075:DNA-directed RNA polymerase, helix hairpin domain;"
MvSl-1064-A1-R4_A1g00049	MvSv-1253-A1-R1_MC12g07670	0	0	PAR	AutoIPR: IPR002761:DUF71 domain; IPR013813:Endoribonuclease L-PSP/chorismate mutase-like;
MvSl-1064-A1-R4_A1g00048	MvSv-1253-A1-R1_MC12g07669	0	0	PAR	
MvSl-1064-A1-R4_A1g00047	MvSv-1253-A1-R1_MC12g07668	0	0	PAR	
MvSl-1064-A1-R4_A1g00046	MvSv-1253-A1-R1_MC12g07667	0	0	PAR	"AutoIPR: IPR011330:Glycoside hydrolase/deacetylase, beta/alpha-barrel;"
MvSl-1064-A1-R4_A1g00044	MvSv-1253-A1-R1_MC12g07665	0	0	PAR	"AutoIPR: IPR011330:Glycoside hydrolase/deacetylase, beta/alpha-barrel;"
MvSl-1064-A1-R4_A1g00040	MvSv-1253-A1-R1_MC12g07664	0	0	PAR	"AutoIPR: IPR011330:Glycoside hydrolase/deacetylase, beta/alpha-barrel;"
MvSl-1064-A1-R4_A1g00039	MvSv-1253-A1-R1_MC12g07663	0	0	PAR	
MvSl-1064-A1-R4_A1g00038	MvSv-1253-A1-R1_MC12g07661	0	0	PAR	

MvSl gene ID (a_1)	MvSv gene ID (a_1)	d_S in MvSl	d_S in MvSv	Stratum	Putative function
MvSl-1064-A1-R4_A1g00037	MvSv-1253-A1-R1_MC12g07660	0	0	PAR	"AutoIPR: IPR001567:Peptidase M3A/M3B; IPR024077:Neurolysin/Thimet oligopeptidase, domain 2; IPR024079:Metallopeptidase, catalytic domain;"
MvSl-1064-A1-R4_A1g00036	MvSv-1253-A1-R1_MC12g07659	0	0	PAR	AutoIPR: IPR006565:Bromodomain transcription factor;This recognition is often a prerequisite for protein-histone association and chromatin remodeling.
MvSl-1064-A1-R4_A1g00035	MvSv-1253-A1-R1_MC12g07658	0	0	PAR	
MvSl-1064-A1-R4_A1g00033	MvSv-1253-A1-R1_MC12g07656	0	0	PAR	
MvSl-1064-A1-R4_A1g00032	MvSv-1253-A1-R1_MC12g07655	0	0	PAR	"AutoIPR: IPR002035:von Willebrand factor, type A;"
MvSl-1064-A1-R4_A1g00031	MvSv-1253-A1-R1_MC12g07654	0	0	PAR	"AutoIPR: IPR003083:S-crystallin; IPR017933:Glutathione S-transferase/chloride channel, C-terminal;"
MvSl-1064-A1-R4_A1g00030	MvSv-1253-A1-R1_MC12g07653	0	0	PAR	
MvSl-1064-A1-R4_A1g00029	MvSv-1253-A1-R1_MC12g07652	0	0	PAR	
MvSl-1064-A1-R4_A1g00009	MvSv-1253-A1-R1_MC12g07644	0	0	PAR	"AutoIPR: IPR006785:Peroxisome membrane anchor protein Pex14p, N-terminal; IPR025655:Peroxisomal membrane protein 14;"
MvSl-1064-A1-R4_A1g00008	MvSv-1253-A1-R1_MC12g07643	0	0	PAR	AutoIPR: IPR013087:Zinc finger C2H2-type/integrase DNA-binding domain;
MvSl-1064-A1-R4_A1g00007	MvSv-1253-A1-R1_MC12g07642	0	0	PAR	AutoIPR: IPR008984:SMAD/FHA domain;
MvSl-1064-A1-R4_A1g00006	MvSv-1253-A1-R1_MC12g07641	0	0	PAR	"AutoIPR: IPR003204:Cytochrome c oxidase, subunit Va/VI;"
MvSl-1064-A1-R4_A1g00005	MvSv-1253-A1-R1_MC12g07640	0	0	PAR	
MvSl-1064-A1-R4_A1g00004	MvSv-1253-A1-R1_MC12g07639	0	0	PAR	AutoIPR: IPR003121:SWIB/MDM2 domain;

Table S4. Raw data summary and assembly statistics for the genomes generated in this study.

sample	Raw data summary							Assembly statistics									
	# Smart cell	# Subreads	Max Subread Length (bp)	N50 (bp)	Mean (bp)	Median (bp)	BP	Accession numbers	# Contigs	Min length (bp)	Max length (bp)	N50 BP	L50 (#contigs)	N90 (bp)	L90 (#contigs)	mean length (bp)	Median Length (bp)	Assembly size (bp)
Microbotryum lagerheimii 1253 A1	4	589978	41394	9526	7290	7059	4 301 220 311	ERS1013677	42	6001	3235273	1584903	7	462124	17	614444	172652	25 806 628
Microbotryum lagerheimii 1253 A2	4	587933	43134	9660	7394	7202	4 347 011 348	ERS1013678	37	7917	3230111	1585144	7	534025	17	693725	474693	25 667 824
Microbotryum violaceum s. str. 1249 A1	4	548702	44168	11951	8759	8361	4 806 182 398	ERS1013671	166	5956	2602331	1183707	10	65951	47	191449	31698	31 780 530
Microbotryum violaceum s. str. 1249 A2	4	456117	46941	13250	9516	8962	4 340 608 458	ERS1013672	61	8455	2644084	1643691	7	606103	17	456993	30510	27 876 544
Microbotryum lychnidis-dioicae Lamole A1	Raw data from Badouin et al. 2015 (12)							ERS1013679	48	12190	3412169	1736850	6	648002	16	622941	44679	29 901 156
Microbotryum lychnidis-dioicae Lamole A2	Raw data from Badouin et al. 2015 (12)							ERS459551	37	15308	4051571	1730088	6	1040457	14	819414	312349	30 318 316
Microbotryum intermedium 1389	3	562278	62677	11040	8512	8220	4 786 123 623	ERS1324257	24	16897	2982376	1644950	6	1002499	13	977543	1002499	23 461 035
Microbotryum silenes-dioicae 1303_A1	7	938931	46274	10834	7946	7576	7 460 889 114	ERS1436592	144	6283	2425171	936137	12	153077	45	233285	32003	33 593 023
Microbotryum silenes-dioicae 1303_A2	6	490924	46480	12620	8406	7474	4 126 642 950	ERS1436593	128	8587	3251277	1321747	10	359665	30	265304	29362	33 958 966

Table S5. *Microbotryum lychnidis-dioicae* and *M. silenes-dioicae* strains used for performing polymorphism analyses. Reference to strain ID, species, mating-type, accession number, number and percentage of reads mapped as proper pairs and reference of the original genome publication, are given.

Strain ID	Species	Mating-type	Accession number	Number of reads mapped as proper pairs	% of reads mapped as proper pairs	Reference
MvSd-335-H3-A1	*M. silenes-dioicae*	a_1	SRS1072004	102696842	96.28%	(48)
MvSd-336-01-A1	*M. silenes-dioicae*	a_1	SRS1072005	127697676	96.85%	(48)
MvSd-578-2-A2	*M. silenes-dioicae*	a_2	SRS1072006|SRS1072007	78559190	96.54%	(48)
MvSd-69-05-A2	*M. silenes-dioicae*	a_2	SRS1072010	121301046	97.35%	(48)
MvSd-707-1-A2	*M. silenes-dioicae*	a_2	SRS1072011	138917854	96.93%	(48)
MvSd-72-A2	*M. silenes-dioicae*	a_2	SRS1072012|SRS1072013	181254142	97.40%	(48)
MvSd-851-6-A2	*M. silenes-dioicae*	a_2	SRS1072015	113257210	97.21%	(48)
MvSd-900-1-A1	*M. silenes-dioicae*	a_1	SRS1072016	143422672	97.33%	(48)
MvSd-932-2-A2	*M. silenes-dioicae*	a_2	SRS1072017	107796114	96.87%	(48)
MvSd-937-2-A2	*M. silenes-dioicae*	a_2	SRS1072018	134111998	97.24%	(48)
MvSd-949-2-A1	*M. silenes-dioicae*	a_1	SRS1072019	105576460	96.66%	(48)
MvSd-IT02-A2	*M. silenes-dioicae*	a_2	SRS1072020	126925450	96.74%	(48)
MvSd-sp002-A1	*M. silenes-dioicae*	a_1	SRS1072021	133835232	96.73%	(48)
MvSd-sp003-A1	*M. silenes-dioicae*	a_1	SRS1072023	110615508	97.32%	(48)
MvSl-00-10-A2	*M. lychnidis-dioicae*	a_2	SRS1072024	71471502	95.32%	(48)
MvSl-100-6-A1	*M. lychnidis-dioicae*	a_1	SRS1072025	70881632	95.69%	(48)
MvSl-140-01-A2	*M. lychnidis-dioicae*	a_2	SRS1072033	157160988	95.07%	(48)
MvSl-141-01-A2	*M. lychnidis-dioicae*	a_2	SRS1072034	66844444	94.89%	(48)
MvSl-40-01-A2	*M. lychnidis-dioicae*	a_2	SRS1072035	65532992	94.18%	(48)
MvSl-446-2-A2	*M. lychnidis-dioicae*	a_2	SRS1072038|SRS1072039	68358472	94.97%	(48)
MvSl-466-3-A1	*M. lychnidis-dioicae*	a_1	SRS1072042|SRS1072043	75508212	94.92%	(48)
MvSl-576-A2	*M. lychnidis-dioicae*	a_2	SRS1072044|SRS1072045	56128954	95.40%	(48)
MvSl-641-A1	*M. lychnidis-dioicae*	a_1	SRS1072046|SRS1072047	87723406	95.25%	(48)
MvSl-661-A2	*M. lychnidis-dioicae*	a_2	SRS1072050	84294192	94.85%	(48)
MvSl-665-A2	*M. lychnidis-dioicae*	a_2	SRS1072048|SRS1072049	37283112	94.87%	(48)
MvSl-687-5-A2	*M. lychnidis-dioicae*	a_2	SRS1072051	46854784	94.81%	(48)
MvSl-830-2-A1	*M. lychnidis-dioicae*	a_1	SRS1072056	81814412	95.81%	(48)
MvSl-856-2-A1	*M. lychnidis-dioicae*	a_1	SRS1072057	37685654	94.57%	(48)
MvSl-I00-3_A2	*M. lychnidis-dioicae*	a_2	SRS1072064	78297378	95.19%	(48)
MvSl-IOA-A1	*M. lychnidis-dioicae*	a_1	SRS1072065	61186726	95.57%	(48)
MvSl-W-1069-A1	*M. lychnidis-dioicae*	a_1	SRS781520	46860062	92.35%	(26)
MvSl-W-1088-A1	*M. lychnidis-dioicae*	a_1	SRS781522	38830336	92.42%	(26)
MvSl-W-1089-A2	*M. lychnidis-dioicae*	a_2	SRS781488	38918966	91.94%	(26)
MvSl-W-1090-A2	*M. lychnidis-dioicae*	a_2	SRS781491	31476556	93.72%	(26)
MvSl-W-1103-A2	*M. lychnidis-dioicae*	a_2	SRS781483	45555798	91.93%	(26)
MvSl-W-405-A1	*M. lychnidis-dioicae*	a_1	SRS780332	88330498	94.39%	(26)
MvSl-W-769-A1	*M. lychnidis-dioicae*	a_1	SRS781521	42520222	91.74%	(26)
MvSl-W-920-A2	*M. lychnidis-dioicae*	a_2	SRS781485	42908076	92.50%	(26)

Table S6. Nucleotide diversity (θ_π) and divergence (mean number of pairwise differences) estimates in pseudo-autosomal regions (PARs) and evolutionary strata in:

(A) *Microbotryum silenes-dioicae*

Gene set	Mean diversity ± SE		Divergence from *M. violaceum s. str*.	
	All sites	Silent sites	All sites	Silent sites
Purple stratum	3.24e-02 ± 1.53e-02	5.23e-02 ± 1.98e-02	4.71e-02 ± 2.04e-02	6.09e-02 ± 1.42e-02
Blue stratum	2.43e-02 ± 1.09e-02	3.72e-02 ± 1.72e-02	5.61e-02 ± 2.09e-02	6.69e-02 ± 1.45e-02
Orange stratum	6.25e-02 ± 4.75e-02	8.88e-02 ± 6.2e-02	7.87e-02 ± 5.16e-02	6.25e-02 ± 2.02e-02
Black stratum	9e-03 ± 8.79e-04	1.45e-02 ± 1.29e-03	2.33e-02 ± 1.13e-03	3.57e-02 ± 1.11e-03
Red stratum	2.47e-03 ± 1.56e-03	4.03e-03 ± 2.41e-03	2.26e-02 ± 3.12e-03	3.88e-02 ± 3.8e-03
Green stratum	2.22e-03 ± 3.6e-04	3.4e-03 ± 8.92e-04	2.39e-02 ± 6.44e-03	4.53e-02 ± 1.27e-02
PARs	2.46e-04 ± 3.37e-05	4.11e-04 ± 8.56e-05	4.1e-02 ± 2.11e-03	8.18e-02 ± 3.54e-03

(B) *Microbotryum lychnidis-dioicae* (whole data set)

Gene set	Mean diversity ± SE		Divergence from *M. violaceum s. str*.	
	All sites	Silent sites	All sites	Silent sites
Purple stratum	3.6e-02 ± 1.48e-02	5.53e-02 ± 2.02e-02	5.28e-02 ± 2.05e-02	6.46e-02 ± 1.47e-02
Blue stratum	2.44e-02 ± 9.91e-03	3.92e-02 ± 1.58e-02	5.66e-02 ± 1.98e-02	7.01e-02 ± 1.39e-02
Orange stratum	6.16e-02 ± 4.51e-02	8.94e-02 ± 6.01e-02	8.06e-02 ± 5.18e-02	6.5e-02 ± 2.04e-02
Black stratum	9.88e-03 ± 6.78e-04	1.61e-02 ± 1.08e-03	2.57e-02 ± 1.02e-03	3.88e-02 ± 1.13e-03
Red stratum	3.11e-03 ± 1.34e-03	3.99e-03 ± 2.36e-03	2.32e-02 ± 2.88e-03	4.03e-02 ± 4.13e-03
Green stratum	1.47e-03 ± 4.39e-04	2.49e-03 ± 1.2e-04	2.48e-02 ± 6.92e-03	4.75e-02 ± 1.12e-02
PARs	2.61e-03 ± 2.22e-04	3.16e-03 ± 2.64e-04	4.41e-02 ± 2.24e-03	8.78e-02 ± 3.79e-03

(C) the North-Western cluster of *Microbotryum lychnidis-dioicae*

Gene set	Mean diversity ± SE		Divergence from *M. violaceum s. str*.	
	All sites	Silent sites	All sites	Silent sites
Purple stratum	3.92e-02 ± 1.61e-02	5.77e-02 ± 2.03e-02	5.23e-02 ± 1.98e-02	6.34e-02 ± 1.36e-02
Blue stratum	2.68e-02 ± 1.09e-02	3.99e-02 ± 1.6e-02	5.69e-02 ± 1.98e-02	7.03e-02 ± 1.38e-02
Orange stratum	6.72e-02 ± 4.95e-02	9.03e-02 ± 6.11e-02	7.8e-02 ± 4.93e-02	6.41e-02 ± 1.93e-02
Black stratum	1.05e-02 ± 7.57e-04	1.63e-02 ± 1.12e-03	2.58e-02 ± 1.02e-03	3.89e-02 ± 1.15e-03
Red stratum	3.4e-03 ± 1.45e-03	4.85e-03 ± 2.41e-03	2.36e-02 ± 2.93e-03	4.07e-02 ± 4.18e-03
Green stratum	4.72e-04 ± 3.69e-04	9.37e-04 ± 9.37e-04	2.5e-02 ± 7.24e-03	4.75e-02 ± 1.22e-02
PARs	9.05e-04 ± 1.23e-04	1.49e-03 ± 2.19e-04	4.45e-02 ± 2.29e-03	8.76e-02 ± 3.79e-03

(D) the Southern cluster of *Microbotryum lychnidis-dioicae*

Gene set	Mean diversity ± SE		Divergence from *M. violaceum s. str*.	
	All sites	Silent sites	All sites	Silent sites
Purple stratum	4.23e-02 ± 1.76e-02	5.54e-02 ± 2e-02	4.73e-02 ± 1.63e-02	5.64e-02 ± 1.07e-02
Blue stratum	2.85e-02 ± 1.18e-02	3.82e-02 ± 1.57e-02	5.66e-02 ± 1.99e-02	6.93e-02 ± 1.36e-02
Orange stratum	7.29e-02 ± 5.34e-02	8.82e-02 ± 5.9e-02	6.26e-02 ± 3.53e-02	5.88e-02 ± 1.41e-02
Black stratum	1.1e-02 ± 8.12e-04	1.54e-02 ± 1.07e-03	2.53e-02 ± 9.53e-04	3.85e-02 ± 1.11e-03
Red stratum	2.8e-03 ± 1.64e-03	3.57e-03 ± 2.24e-03	2.35e-02 ± 3.16e-03	4.01e-02 ± 4.28e-03
Green stratum	8.3e-04 ± 5.2e-04	1.2e-03 ± 1.2e-03	2.5e-02 ± 6.54e-03	4.81e-02 ± 9.62e-03
PARs	1.07e-03 ± 1.29e-04	1.66e-03 ± 2.58e-04	4.39e-02 ± 2.19e-03	8.71e-02 ± 3.78e-03

Table S7. Results of maximum-likelihood Hudson-Kreitman-Agade (MLHKA) tests for assessing whether differences in diversity between each evolutionary stratum and the pseudo-autosomal regions (PARs) is due to balancing selection or elevated mutation rates. Genes were concatenated per stratum unless specified otherwise. Statistically significant results before and after correction for multiple testing at the significance level of 0.05 are indicated in bold; d.f.: degrees of freedom; Selection coefficient: maximum likelihood estimate of the selection coefficient.

(A) In *Microbotryum silenes-dioicae*

Test	d.f.	Selection coefficient	ln likelihood null model	ln likelihood alternative model	Chi2 statistics	p-values	Adjusted p-values
Purple stratum vs PAR	1	60.4123	-284.798	-370.048	170.5	**5.75e-39**	**4.03e-38**
Blue stratum vs PAR	1	44.6019	-286.815	-370.684	167.74	**2.31e-38**	**1.38e-37**
Orange stratum vs PAR	1	75.4768	-286.583	-391.715	210.26	**1.20e-47**	**9.62e-47**
Black stratum vs PAR	1	24.844	-287.805	-340.116	104.62	**1.48e-24**	**7.39e-24**
Red stratum vs PAR	1	7.6661	-288.224	-300.015	23.58	**1.20e-06**	**3.59e-06**
Green stratum vs PAR	1	4.74454	-285.191	-289.094	7.81	**5.21e-03**	**5.21e-03**
Red stratum vs PAR (no concatenation)	16	56.0665	-335.885	-380.386	89	**3.82e-12**	**1.53e-11**
Green stratum vs PAR (no concatenation)	3	10.3826	-289.177	-297.46	16.57	**8.68e-04**	**1.74e-03**

(B) In *Microbotryum lychnidis-dioicae* (whole data set)

Test	d.f.	Selection coefficient	ln likelihood null model	ln likelihood alternative model	Chi2 statistics	p-values	Adjusted p-values
Purple stratum vs PAR	1	12.1267	-383.916	-412.85	57.87	**2.80e-14**	**1.40e-13**
Blue stratum vs PAR	1	10.7939	-386.523	-412.316	51.59	**6.85e-13**	**2.74e-12**
Orange stratum vs PAR	1	18.0431	-384.52	-424.17	79.3	**5.34e-19**	**3.20e-18**
Black stratum vs PAR	1	6.39375	-385.591	-402.312	33.44	**7.34e-09**	**2.20e-08**
Red stratum vs PAR	1	1.94212	-383.672	-385.361	3.38	6.61e-02	1.32e-01
Green stratum vs PAR	1	0.795155	-384.517	-380.695	-7.64	1.00e+00	1.00e+00

(C) In the North-Western cluster of *Microbotryum lychnidis-dioicae*

Test	d.f.	Selection coefficient	ln likelihood null model	ln likelihood alternative model	Chi2 statistics	p-values	Adjusted p-values
Red stratum vs PAR	1	4.96955	-344.795	-336.841	15.91	**6.65e-05**	**1.99e-04**
Green stratum vs PAR	1	0.941793	-333.064	-336.68	-7.23	1.00e+00	1.00e+00
Red stratum vs PAR (no concatenation)	16	2.29673	-417.742	-388.587	58.31	**1.01e-06**	**4.02e-06**
Green stratum vs PAR (no concatenation)	3	0	-332.85	-333.992	-2.28	1.00e+00	1.00e+00

(D) In the Southern cluster of *Microbotryum lychnidis-dioicae*

Test	d.f.	Selection coefficient	ln likelihood null model	ln likelihood alternative model	Chi2 statistics	p-values	Adjusted p-values
Red stratum vs PAR	1	4.0771	-348.271	-341.431	13.68	**2.17e-04**	**8.67e-04**
Green stratum vs PAR	1	1.1329	-339.258	-342.942	-7.37	1.00e+00	1.00e+00
Red stratum vs PAR (no concatenation)	16	1.48588	-410.369	-392.762	32.65	**8.22e-03**	**2.46e-02**
Green stratum vs PAR (no concatenation)	3	0.639097	-338.134	-342.151	-8.03	1.00e+00	1.00e+00